# Supporting Information

## Cyclization or bridging, which is faster is the key in the self-assembly mechanism of $Pd_6L_3$ coordination prisms

Xinman Zhang,[¶,a,] Satoshi Takahashi,[¶,a] Keisuke Aratsu,[a] Isamu Kikuchi,[a] Hirofumi Sato,[b,c,d] and Shuichi Hiraoka*[a]

[¶] These authors equally contributed to this research.
[a]Department of Basic Science, Graduate School of Arts and Sciences, The University of Tokyo, 3-8-1 Komaba, Meguro-ku, Tokyo 153-8902, Japan
[b]Department of Molecular Engineering, Kyoto University, Kyoto 615-8510, Japan
[c]Elements Strategy Initiative for Catalysts and Batteries, Kyoto University, Kyoto 615-8510, Japan
[d]Fukui Institute for Fundamental Chemistry, Kyoto University, Kyoto 606-8103, Japan

E-mail: hiraoka-s@g.ecc.u-tokyo.ac.jp

**Contents**

## General Information

$^1$H and $^{19}$F NMR spectra were recorded using a Bruker AV-500 (500 MHz) spectrometer. All $^1$H spectra were referenced using a residual solvent peak, $CD_3NO_2$ (δ 4.33), $CDCl_3$ (δ 7.26), and $CD_3OD$ (δ 3.31). Electrospray ionization time-of-flight (ESI-TOF) mass spectra were obtained using a Waters Xevo G2-S Tof mass spectrometer.

## Materials

Unless otherwise noted, all solvents and reagents were obtained from commercial suppliers (TCI Co., Ltd., WAKO Pure Chemical Industries Ltd., KANTO Chemical Co., Inc., and Sigma-Aldrich Co.) and were used as received. $CD_3NO_2$ was purchased from Acros Organics and used after dehydration with Molecular Sieves 4Å. Tetratopic ligands **1**[1] and **2**[2], $[Pd(TMEDA)Py^*_2](BF_4)_2$[3], and $[Pd(TMEDA)Py^*_2](BArF)_2$[4] were prepared according to the literature.

## Negative allosteric cooperativity of the tetratopic ligands

### Determination of the protonation constants of the tetratopic ligands (**1** and **2**)

The protonation of a tetratopic ligand (L) is expressed by the following four equilibria.

$$L + H^+ \rightleftarrows LH \quad (1)$$
$$LH + H^+ \rightleftarrows LH_2 \quad (2)$$
$$LH_2 + H^+ \rightleftarrows LH_3 \quad (3)$$
$$LH_3 + H^+ \rightleftarrows LH_4 \quad (4)$$

where the charge(s) in the protonate ligands, LH, $LH_2$, $LH_3$, and $LH_4$, are omitted for the sake of simplicity. The equilibrium constants for these equilibria are defined as follows:

$$K_i = \frac{[\mathrm{LH}_i]}{[\mathrm{LH}_{i-1}][\mathrm{H}^+]} \quad (i = 1\text{–}4) \quad (5)$$

The total concentrations of L and proton, $[L]_0$ and $[H^+]_0$, in each titration are expressed by equations (6) and (7), respectively.

$$[L]_0 = [L] + [LH] + [LH_2] + [LH_3] + [LH_4] \quad (6)$$
$$[H^+]_0 = [H^+] + [LH] + 2[LH_2] + 3[LH_3] + 4[LH_4] \quad (7)$$

The concentration of proton that binds to the binding sites, $N_{H+}$, can be expressed by equation (8).

$$N_{H+} = [LH] + 2[LH_2] + 3[LH_3] + 4[LH_4] = [H^+]_0 - [H^+] \quad (8)$$

The average occupation of the binding sites in the tetratopic ligand, L, with proton(s) is indicated as $N_{H+}/(4\cdot[L]_0)$.

$$\text{The occupation ratio of the binding sites} = \frac{N_{\mathrm{H+}}}{4\cdot[\mathrm{L}]_0} \quad (9)$$

The average occupation of the binding sites in L can be determined by the chemical shift change of the signals of the tetratopic ligand, $\Delta\delta_{obs}/\Delta\delta_{full}$.

$$\frac{N_{\mathrm{H+}}}{4\cdot[\mathrm{L}]_0} = \frac{\Delta\delta_{obs}}{\Delta\delta_{full}} \quad (10)$$

where $\Delta\delta_{obs}$ is the chemical shift change of the signal of the tetratopic ligand L upon addition of a certain amount of proton (TFA), while $\Delta\delta_{full}$ indicates the chemical shift change when all the binding sites in L are fully protonated. Using these equations, $[L]_0/([H^+]_0 - [H^+])$ can be expressed by equation (11).

$$[L]_0/([H^+]_0 - [H^+]) = (K_1^{-1}\cdot K_2^{-1}\cdot K_3^{-1}\cdot K_4^{-1}\cdot [H^+]^{-4} + K_2^{-1}\cdot K_3^{-1}\cdot K_4^{-1}\cdot[H^+]^{-3} + K_3^{-1}\cdot K_4^{-1}\cdot[H^+]^{-2} + K_4^{-1}\cdot[H^+]^{-1} + 1)/(K_2^{-1}\cdot K_3^{-1}\cdot K_4^{-1}\cdot[H^+]^{-3} + 2\cdot K_3^{-1}\cdot K_4^{-1}\cdot[H^+]^{-2} + 3\cdot K_4^{-1}\cdot[H^+]^{-1} + 4) \quad (11)$$

Therefore, when $[L]_0$, $[H^+]_0$, $K_1$, $K_2$, $K_3$, and $K_4$ are given, the concentration of free proton, $[H^+]$, can be numerically calculated from equation (11), so the occupation ratio of the binding sites in the tetratopic ligand, $([H^+]_0 - [H^+])/(4\cdot[L]_0)$, is determined. The best $K_1$, $K_2$, $K_3$, and $K_4$ were determined by least-squares method

for the difference between the experimental and numerical average occupation values, $\Delta\delta_{obs}/\Delta\delta_{full}$ and $([H^+]_0 - [H^+])/(4\cdot[L]_0)$.

### Titration experiment of the tetratopic ligands with TFA

A 2.4 mM solution of [2.2]paracyclophane in $CHCl_3$ (125 mL), which was used as an internal standard, was added to two NMR tubes (tubes **I** and **II**) and the solvent was removed in vacuo. A solution of tetratopic ligand **1** (0.75 mM) in $CHCl_3$ (400 mL) was added to tube **I** and a solution of tetratopic ligand **2** (3 mM) in $CHCl_3$ (100 mL) was added to tube **II**, and the solvent was removed in vacuo. Then $CDCl_3$ (160 mL) and $CD_3OD$ (320 mL) were added to tubes **I** and **II** and the exact amounts of **1** and **2** in tubes **I** and **II** were determined through the comparison of the signal intensity with [2.2]paracyclophane by $^1$H NMR. A solution of TFA (200 mM) in $CDCl_3$ and $CD_3OD$ (1:2, v/v) was prepared (solution **A**). Solution **A** was gradually added to tubes **I** and **II**, and the protonation was monitored at 298 K by $^1$H NMR spectroscopy. The $^1$H NMR spectra for the titration experiments for **1** and **2** with TFA are shown in Figures S1 and S2, respectively. The experimental binding isotherms, the fitting data, and the protonation constants determined for the two ligands are shown in Figure S3. In the case where the protonation constant of the fourth binding sites ($K_4$) is very small, high concentration of the ligand is needed to accurately determine $\Delta\delta_{full}$. However, because of low solubility of **1** and **2** in a variety solvent, such experiments could not be conducted. Therefore, experimental data obtained at the end of the titration ($[H^+]_0/[L]_0 > 200$) were not used for the fitting. Though there is some uncertainty in the protonation constants (especially $K_4$) for **1** and **2** determined here, as shown in Figure S3 both the two ligands have strong negative allosteric cooperativity.

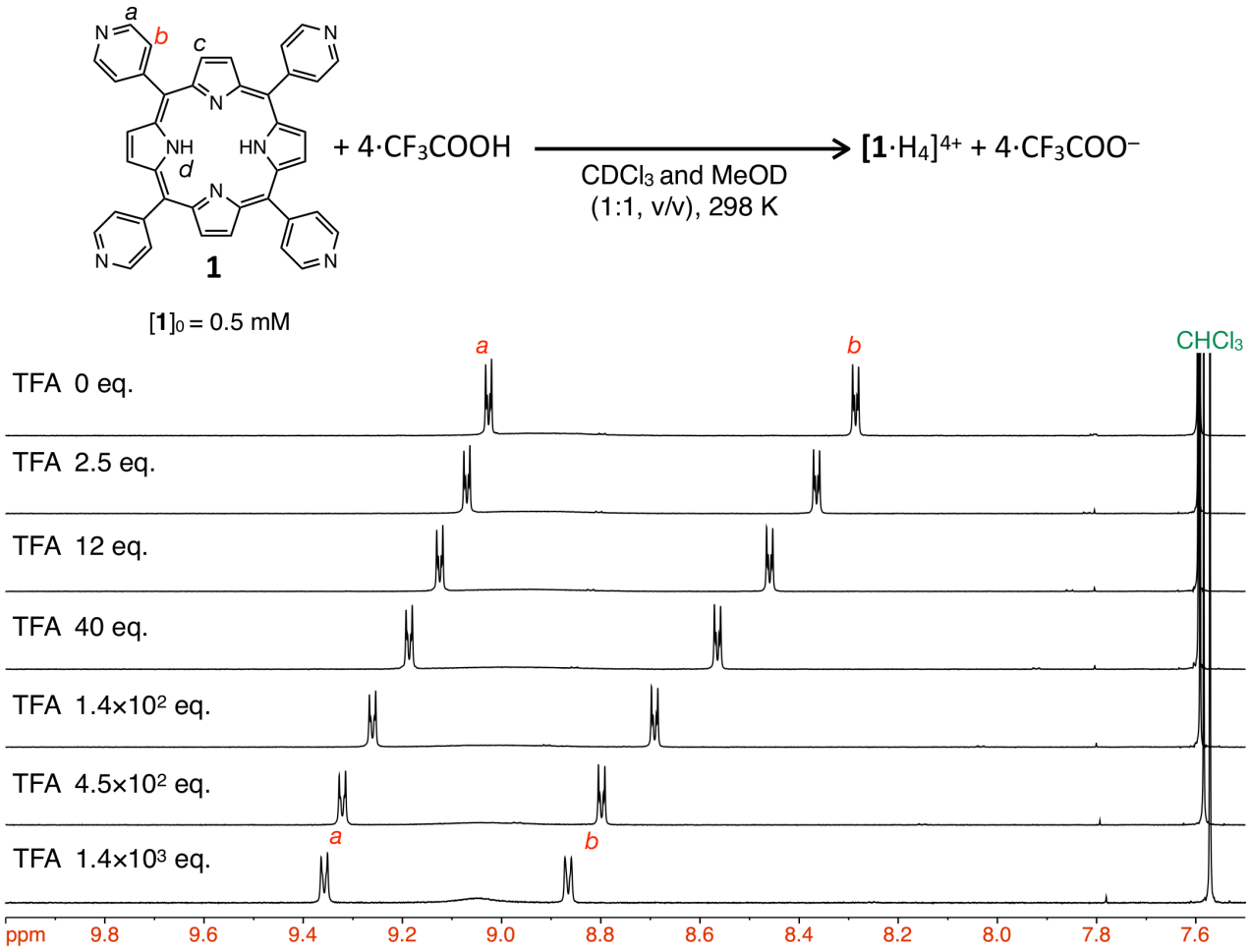


**Figure S1.** $^1$H NMR spectra (500 MHz, $CDCl_3$ and $CD_3OD$ (1:1, v/v), 298 K) for the titration of the tetratopic ligand **1** with TFA (initial $[\mathbf{1}]_0$ = 0.5 mM).

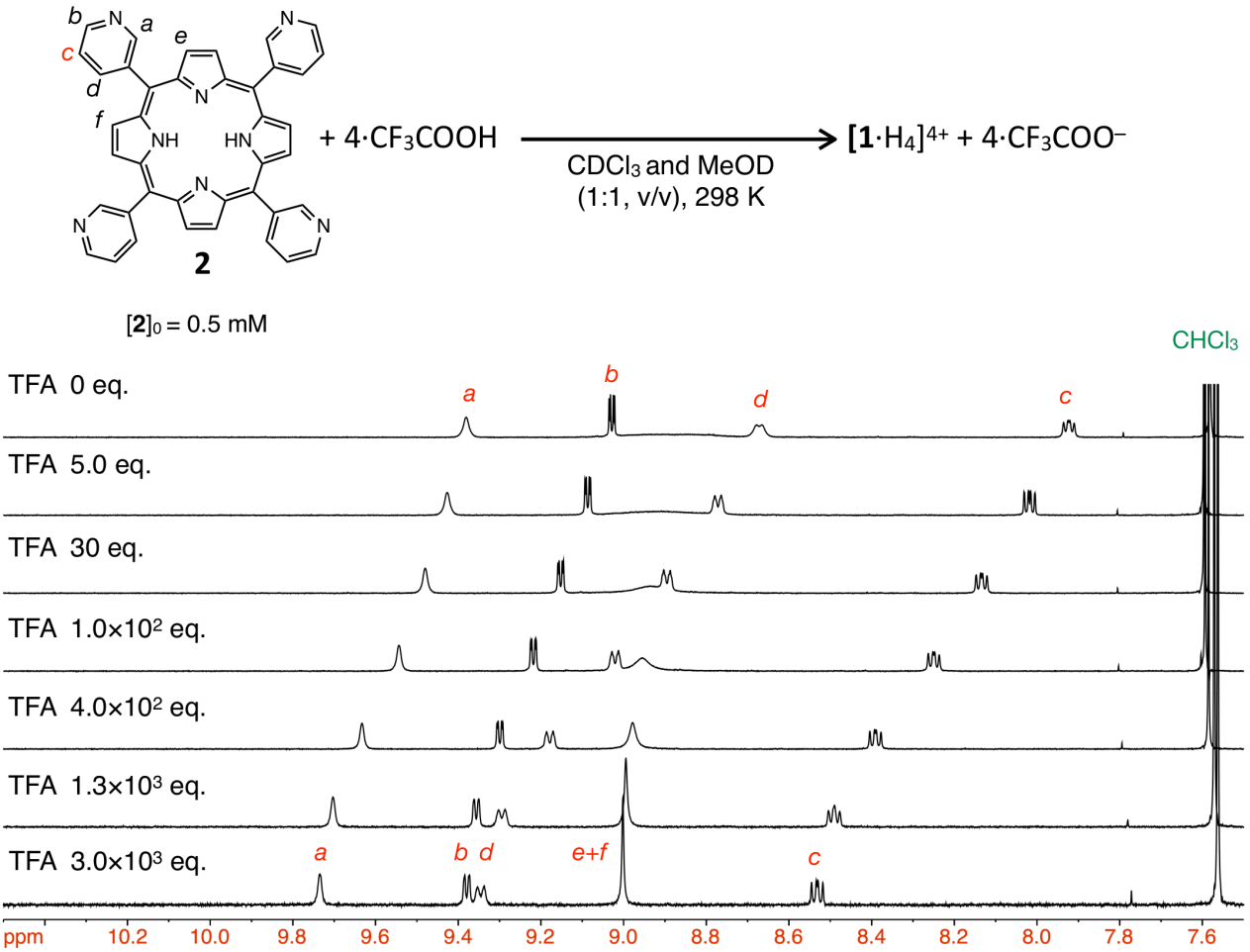


**Figure S2.** $^1$H NMR spectra (500 MHz, $CDCl_3$ and $CD_3OD$ (1:1, v/v), 298 K) for the titration of the tetratopic ligand **2** with TFA (initial $[\mathbf{2}]_0$ = 0.5 mM).

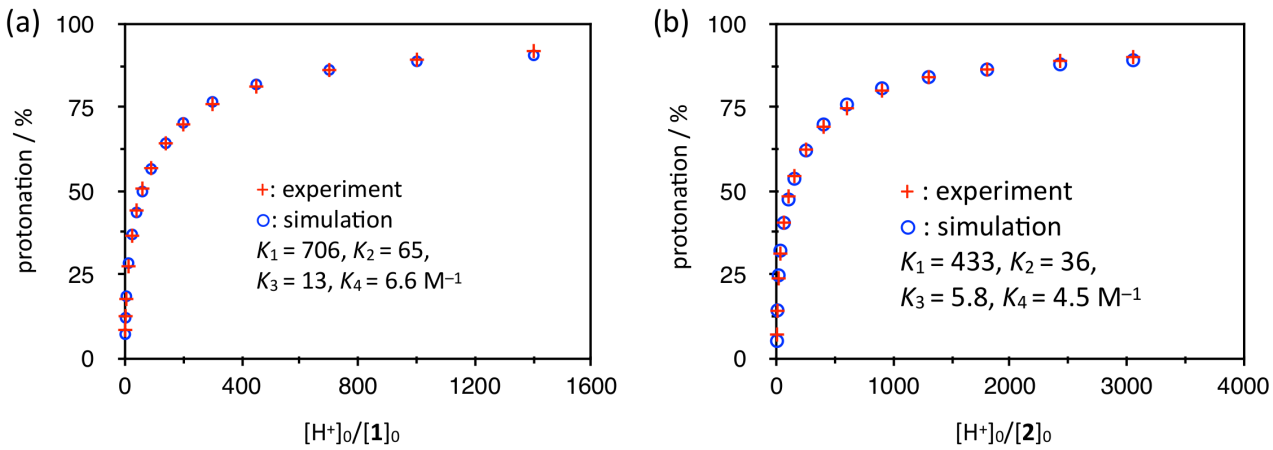


**Figure S3.** The binding isotherms for the protonation of the tetratopic ligands **1** (a) and **2** (b) with TFA. The values of the residual sum of squares (RSS) and the root mean square (RMS) between the experimental and simulation data for total of 15 sample points are given as follows: For **1**, RSS = 7.70, RMS = 0.72; For **2**, RSS = 11.0, RMS = 0.86.

## Monitoring the self-assembly of the $[\boldsymbol{Pd}_6L_3]^{12+}$ prisms by $^1$H NMR spectroscopy

### Procedure for monitoring the self-assembly process of the $[\boldsymbol{Pd}_6\mathbf{1}_3](BArF)_{12}$ prism

A 2.4 mM solution of [2.2]paracyclophane in $CHCl_3$ (125 μL), which was used as an internal standard, was added to two NMR tubes (tubes **I** and **II**) and the solvent was removed in vacuo. A solution of $[\boldsymbol{Pd}Py^*_2](BArF)_2$ (***Pd*** indicates Pd(TMEDA)) (12 mM) in $CD_3NO_2$ was prepared (solution **A**). Solution **A** (50 μL) and $CD_3NO_2$ (500 μL) were added to tube **I**. The exact concentration of $[\boldsymbol{Pd}Py^*_2](BArF)_2$ in solution **A** was determined through the comparison of the integral of the signal for $[\boldsymbol{Pd}Py^*_2](BArF)_2$ with that for [2.2]paracyclophane by $^1$H NMR. A solution of the tetratopic ligand **1** (0.75 mM) in $CHCl_3$ (400 μL) was added to tube **II** and the solvent was removed in vacuo. Then $CDCl_3$ (500 μL) was added to tube **II** and the exact amount of **1** in tube **II** was determined through the comparison of the integral of the signal for **1** with that for [2.2]paracyclophane by $^1$H NMR. Then the solvent in tube **II** was removed in vacuo, and $CDCl_3$ (200 μL) and $CD_3NO_2$ (350 μL) were added to tube **II**. 2.00 eq. (against the amount of the ligand **1** in tube **II**) of solution **A** (*ca.* 50 μL; the exact amount was determined based on the exact concentration of solution **A** and the amount of **1** in tube **II**) were added to tube **II** at 298 K. The self-assembly of the $[\boldsymbol{Pd}_6\mathbf{1}_3](BArF)_{12}$ prism was monitored at 298 K by $^1$H NMR spectroscopy until 12 h. Examples of the $^1$H NMR spectra are shown in Figure 3a. The exact ratio of **1** and $[\boldsymbol{Pd}Py^*_2](BArF)_2$ was unambiguously determined by the integral values of them based on that of [2.2]paracyclophane. The amounts of **1**, $[\boldsymbol{Pd}Py^*_2](BArF)_2$, $[\boldsymbol{Pd}_6\mathbf{1}_3](BArF)_{12}$, and Py* were quantified by the integral value of each $^1$H signal against the signal of the internal standard ([2.2]paracyclophane). To confirm the reproducibility, the same experiment was carried out three times (runs 1–3). The average values of the existence ratios and the ($\langle n\rangle$, $\langle k\rangle$) values are listed in Tables S1–S5.

### Procedure for monitoring the self-assembly process of the $[\boldsymbol{Pd}_6\mathbf{2}_3](BF_4)_{12}$ prism

A 2.4 mM solution of [2.2]paracyclophane in $CHCl_3$ (125 μL), which was used as an internal standard, was added to two NMR tubes (tubes **I** and **II**) and the solvent was removed in vacuo. A solution of $[\boldsymbol{Pd}Py^*_2](BF_4)_2$ (24 mM) in $CD_3NO_2$ was prepared (solution **A**). Solution **A** (50 μL) and $CD_3NO_2$ (500 μL) were added to tube **I**. The exact concentration of $[\boldsymbol{Pd}Py^*_2](BF_4)_2$ in solution **A** was determined through the comparison of the integrals of its signal with that of [2.2]paracyclophane by $^1$H NMR. A solution of the tetratopic ligand **2** (6 mM) in $CHCl_3$ (100 μL) was added to tube **II** and the solvent was removed in vacuo. Then $CDCl_3$ (120 μL) and $CD_3NO_2$ (430 μL) were added to tube **II** and the exact amount of **2** in tube **II** was determined by its integral values based on [2.2]paracyclophane by $^1$H NMR. 2.00 eq. (against the amount of the ligand **2** in tube **II**) of solution **A** (*ca.* 50 μL; the exact amount was determined based on the exact concentration of solution **A** and the amount of **2** in tube **II**) were added to tube **II** at 263 K. The self-assembly of the $[\boldsymbol{Pd}_6\mathbf{2}_3](BF_4)_{12}$ prism was monitored at 298 K by $^1$H NMR spectroscopy until 36 h, since then the reaction mixture was heated at 333 K and monitored at 298 K by $^1$H NMR spectroscopy. Examples of the $^1$H NMR spectra are shown in Figures 3b and S4. The exact ratio of **2** and $[\boldsymbol{Pd}Py^*_2](BF_4)_2$ was unambiguously determined by the comparison of the integral value of each $^1$H signal of [2.2]paracyclophane. The amounts of **2**, $[\boldsymbol{Pd}Py^*_2](BF_4)_2$, $[\boldsymbol{Pd}_6\mathbf{2}_3](BF_4)_{12}$, and Py* were quantified by the integral value of each $^1$H signal against the signal of the internal standard ([2.2]paracyclophane). In order to confirm the reproducibility, the same experiment was carried out three times (runs 1–3). The average values of the existence ratios and the ($\langle n\rangle$, $\langle k\rangle$) values are listed in Tables S6–S10.

### Determination of the existence ratio of each species

The relative integral value of each $^1$H NMR signal against the internal standard [2.2]paracyclophane is used as the integral value in this description. We define the integral values of the signal for the substrates and the products at each time $t$ as follows:

For the self-assembly of the $[\boldsymbol{Pd}_6\mathbf{1}_3](BArF)_{12}$ prism from $[\boldsymbol{Pd}Py^*_2](BArF)_2$ and **1**:
$I_L(t)$: As **1** has eight $a$ hydrogens, 1/8 of the integral value of $a$ proton in the free tetratopic ligand **1**
$I_M(t)$: the integral value of the $i$ proton of Py* in $[\boldsymbol{Pd}Py^*_2](BArF)_2$
$I_{\mathbf{prism}}(t)$: As **1** in in the $[\boldsymbol{Pd}_6\mathbf{1}_3]^{12+}$ prism has four $a_1$ hydrogens, 1/4 of the integral value of the $a_1$ proton in the $[\boldsymbol{Pd}_6\mathbf{1}_3](BArF)_{12}$ prism
$I_{Py^*}(t)$: the integral value of the $h$ proton of free Py*
(see Figure 2a to ensure the signal assignment for the self-assembly of the $[\boldsymbol{Pd}_6\mathbf{1}_3](BArF)_{12}$ prism)

For the self-assembly of the $[\boldsymbol{Pd}_6\mathbf{2}_3](BF_4)_{12}$ prism from $[\boldsymbol{Pd}Py^*_2](BF_4)_2$ and **2**:
$I_L(t)$: As **2** has four $l$ hydrogens, 1/4 of the integral value of the $l$ proton in free ligand **2**
$I_M(t)$: the integral value of the $h$ proton of Py* in $[\boldsymbol{Pd}Py^*_2](BF_4)_2$

$I_{\mathbf{prism}}(t)$: As **2** in the $[\boldsymbol{Pd}_6\mathbf{2}_3]^{12+}$ prism has four $k$ hydrogens, 1/4 of the integral value of the $k$ proton in the $[\boldsymbol{Pd}_6\mathbf{2}_3](BF_4)_{12}$ prism
$I_{Py*}(t)$: the integral value of the $h$ proton of free Py*
(see Figure 2b to ensure the signal assignment for the self-assembly of the $[\boldsymbol{Pd}_6\mathbf{2}_3](BF_4)_{12}$ prism)

$I_M(0)$ was determined based on the exact concentration of solution **A** determined by $^1$H NMR and the exact volume of solution **A** added into tube **II**.
$I_L(0)$ was determined by $^1$H NMR measurement before the addition of solution **A** into tube **II**.

<u>Existence ratio of $[\boldsymbol{Pd}Py*_2]^{2+}$</u>
As the total amount of $[\boldsymbol{Pd}Py*_2]^{2+}$ corresponds to $I_M(0)$, the existence ratio of $[\boldsymbol{Pd}Py*_2]^{2+}$ at $t$ is expressed by $I_M(t)/I_M(0)$.

<u>Existence ratio of L</u>
As the total amount of free ligand L corresponds to $I_L(0)$, the existence ratio of L at $t$ is expressed by $I_L(t)/I_L(0)$.

<u>Existence ratio of Py*</u>
As the total amount of Py* corresponds to $I_M(0)$, the existence ratio of Py* at $t$ is expressed by $I_{Py*}(t)/I_M(0)$.

<u>Existence ratio of $[\boldsymbol{Pd}_6L_3]^{12+}$</u>
As the $[\boldsymbol{Pd}_6L_3]^{12+}$ prism is quantified based on L, the existence ratio of $[\boldsymbol{Pd}_6L_3]^{12+}$ at $t$ is expressed by $I_{\mathbf{prism}}(t)/I_L(0)$.

<u>Existence ratio of the total intermediates (**Int**)</u>
The existence ratio of the total intermediates (**Int**) is determined based on the amount of ligand L in the intermediates. Thus, the existence ratio of **Int** is calculated by subtracting the other species containing L (free L, $[\boldsymbol{Pd}_6L_3]^{12+}$) from the total amount of L ($I_L(0)$). The existence ratio of **Int** at $t$ is expressed by $(I_L(0) - I_L(t) - I_{prism}(t))/I_L(0)$.

$\langle a \rangle$
The total amount of $Pd^{2+}$ ions corresponds to $I_M(0)/2$. The amount of $Pd^{2+}$ ions in $[\boldsymbol{Pd}Py*_2]^{2+}$ at $t$ corresponds to $I_M(t)/2$. The amount of $Pd^{2+}$ ions in prism at $t$ corresponds to $I_{prism}(t)\times 2$. The amount of $Pd^{2+}$ ions in **Int** at $t$ is thus expressed by $I_M(0)/2 - I_M(t)/2 - I_{prism}(t)\times 2$.

$\langle b \rangle$
The total amount of ligand L corresponds to $I_L(0)$. The amount of free ligand L at $t$ corresponds to $I_L(t)$. The amounts of ligand L in prism at $t$ corresponds to $I_{prism}(t)$. The amount of ligand L in **Int** at $t$ is thus expressed by $I_L(0) - I_L(t) - I_{prism}(t)$.

$\langle c \rangle$
The total amount of Py* corresponds to $I_M(0)$. The amount of free Py* at $t$ corresponds to $I_{Py*}(t)$. The amount of Py* in $[\boldsymbol{Pd}Py*_2]^{2+}$ at $t$ corresponds to $I_M(t)$. The amount of Py* in **Int** at $t$ is thus expressed by $I_M(0) - I_{Py*}(t) - I_M(t)$.

The $\langle n \rangle$ and $\langle k \rangle$ values are determined with these $\langle a \rangle$, $\langle b \rangle$, and $\langle c \rangle$ values by eqs. (12) and (13).

$$\langle n \rangle = \frac{2\langle a \rangle - \langle c \rangle}{\langle b \rangle} \quad (12)$$

$$\langle k \rangle = \frac{\langle a \rangle}{\langle b \rangle} \quad (13)$$

Time variation of **1**, [***Pd***Py*$_2$](BArF)$_2$, [***Pd***$_6$**1**$_3$](BArF)$_{12}$, Py*, **Int**, and the (⟨*n*⟩, ⟨*k*⟩) values for the self-assembly of the [***Pd***$_6$**1**$_3$](BArF)$_{12}$ prism (Tables S1–S5)

**Table S1.** Average time variation of **1**, [***Pd***Py*$_2$](BArF)$_2$, [***Pd***$_6$**1**$_3$](BArF)$_{12}$, Py*, and **Int**; ⟨*a*⟩–⟨*c*⟩ values of the average composition of the intermediates (***Pd***$_{\langle a\rangle}$**1**$_{\langle b\rangle}$Py*$_{\langle c\rangle}$); (⟨*n*⟩, ⟨*k*⟩) values for the self-assembly of [***Pd***$_6$**1**$_3$](BArF)$_{12}$ from **1** and [***Pd***Py*$_2$](BArF)$_2$ in $CD_3NO_2$ and $CDCl_3$ (2:1, v/v) at 298 K ([**1**]$_0$ = *ca* 0.5 mM).

| Time / min | **1** / % | [***Pd***Py*$_2$](BArF)$_2$ / % | ***Pd***$_6$**1**$_3$ / % | Py* / % | **Int** / % | ⟨*a*⟩ | ⟨*b*⟩ | ⟨*c*⟩ | ⟨*n*⟩ | ⟨*k*⟩ |
|---|---|---|---|---|---|---|---|---|---|---|
| 0 | 100.0 | 100.0 | 0.0 | 0.0 | 0.0 | — | — | — | — | — |
| 5 | 0.0 | 51.7 | 0.4 | 35.8 | 99.6 | 0.098 | 0.099 | 0.053 | 1.463 | 0.988 |
| 10 | 0.0 | 47.0 | 2.8 | 39.7 | 97.2 | 0.103 | 0.096 | 0.056 | 1.563 | 1.063 |
| 15 | 0.0 | 43.9 | 4.7 | 42.9 | 95.3 | 0.106 | 0.094 | 0.056 | 1.656 | 1.111 |
| 20 | 0.0 | 41.5 | 6.0 | 45.6 | 94.0 | 0.108 | 0.093 | 0.055 | 1.742 | 1.152 |
| 25 | 0.0 | 39.5 | 7.8 | 47.3 | 92.2 | 0.109 | 0.091 | 0.056 | 1.772 | 1.181 |
| 30 | 0.0 | 37.9 | 9.1 | 48.9 | 90.9 | 0.109 | 0.090 | 0.056 | 1.812 | 1.204 |
| 35 | 0.0 | 37.3 | 10.7 | 50.2 | 89.3 | 0.107 | 0.089 | 0.053 | 1.832 | 1.203 |
| 40 | 0.0 | 36.3 | 11.7 | 51.2 | 88.3 | 0.108 | 0.088 | 0.052 | 1.859 | 1.218 |
| 45 | 0.0 | 35.7 | 13.0 | 52.8 | 87.0 | 0.106 | 0.086 | 0.049 | 1.902 | 1.221 |
| 50 | 0.0 | 35.2 | 14.1 | 52.5 | 85.9 | 0.105 | 0.085 | 0.053 | 1.858 | 1.223 |
| 55 | 0.0 | 34.8 | 15.4 | 53.8 | 84.6 | 0.103 | 0.084 | 0.048 | 1.893 | 1.221 |
| 60 | 0.0 | 34.4 | 16.1 | 54.2 | 83.9 | 0.103 | 0.083 | 0.048 | 1.892 | 1.222 |
| 120 | 0.0 | 31.2 | 26.8 | 59.6 | 73.2 | 0.089 | 0.073 | 0.040 | 1.886 | 1.197 |
| 180 | 0.0 | 29.8 | 34.4 | 63.2 | 65.6 | 0.076 | 0.065 | 0.031 | 1.867 | 1.147 |
| 240 | 0.0 | 29.5 | 38.7 | 63.9 | 61.3 | 0.068 | 0.061 | 0.029 | 1.758 | 1.097 |
| 300 | 0.0 | 29.2 | 44.3 | 66.6 | 55.7 | 0.058 | 0.055 | 0.024 | 1.655 | 1.019 |
| 360 | 0.0 | 28.0 | 46.8 | 66.4 | 53.2 | 0.055 | 0.053 | 0.026 | 1.585 | 1.021 |
| 420 | 0.0 | 27.8 | 49.9 | 67.4 | 50.1 | 0.049 | 0.050 | 0.025 | 1.470 | 0.968 |
| 480 | 0.0 | 27.3 | 52.4 | 68.5 | 47.6 | 0.045 | 0.047 | 0.023 | 1.436 | 0.937 |
| 540 | 0.0 | 26.9 | 55.1 | 68.8 | 44.9 | 0.041 | 0.044 | 0.024 | 1.287 | 0.890 |
| 720 | 0.0 | 25.8 | 59.7 | 70.4 | 40.3 | 0.034 | 0.040 | 0.022 | 1.151 | 0.815 |

**Table S2.** Standard errors for each time point of **1**, [***Pd***Py*$_2$](BArF)$_2$, [***Pd***$_6$**1**$_3$](BArF)$_{12}$, Py*, and **Int**; ⟨*a*⟩–⟨*c*⟩ values of the average composition of the intermediates (***Pd***$_{\langle a\rangle}$**1**$_{\langle b\rangle}$Py*$_{\langle c\rangle}$); (⟨*n*⟩, ⟨*k*⟩) values for the self-assembly of [***Pd***$_6$**1**$_3$](BArF)$_{12}$ from **1** and [***Pd***Py*$_2$](BArF)$_2$ in $CD_3NO_2$ and $CDCl_3$ (2:1, v/v) at 298 K ([**1**]$_0$ = *ca* 0.5 mM).

| Time / min | **1** / % | [***Pd***Py*$_2$](BArF)$_2$ / % | ***Pd***$_6$**1**$_3$ / % | Py* / % | **Int** / % | ⟨*a*⟩ | ⟨*b*⟩ | ⟨*c*⟩ | ⟨*n*⟩ | ⟨*k*⟩ |
|---|---|---|---|---|---|---|---|---|---|---|
| 0 | 0.00 | 0.00 | 0.00 | 0.00 | 0.00 | — | — | — | — | — |
| 5 | 0.00 | 3.12 | 0.43 | 0.78 | 0.43 | 0.014 | 0.008 | 0.019 | 0.028 | 0.066 |
| 10 | 0.00 | 3.38 | 0.36 | 0.72 | 0.36 | 0.013 | 0.007 | 0.019 | 0.042 | 0.064 |
| 15 | 0.00 | 3.84 | 0.38 | 0.84 | 0.38 | 0.015 | 0.007 | 0.020 | 0.037 | 0.082 |
| 20 | 0.00 | 3.39 | 0.31 | 0.41 | 0.31 | 0.015 | 0.007 | 0.018 | 0.018 | 0.072 |
| 25 | 0.00 | 3.33 | 0.32 | 0.70 | 0.32 | 0.015 | 0.007 | 0.018 | 0.034 | 0.072 |
| 30 | 0.00 | 3.31 | 0.58 | 0.63 | 0.58 | 0.015 | 0.007 | 0.018 | 0.027 | 0.075 |
| 35 | 0.00 | 3.20 | 0.58 | 0.67 | 0.58 | 0.014 | 0.007 | 0.018 | 0.030 | 0.072 |
| 40 | 0.00 | 2.95 | 0.52 | 0.93 | 0.52 | 0.014 | 0.007 | 0.016 | 0.047 | 0.068 |
| 45 | 0.00 | 3.01 | 0.87 | 0.98 | 0.87 | 0.015 | 0.007 | 0.017 | 0.044 | 0.074 |
| 50 | 0.00 | 2.71 | 0.78 | 1.06 | 0.78 | 0.014 | 0.007 | 0.017 | 0.046 | 0.065 |
| 55 | 0.00 | 2.66 | 1.08 | 1.03 | 1.08 | 0.014 | 0.007 | 0.017 | 0.039 | 0.070 |
| 60 | 0.00 | 2.43 | 1.12 | 1.11 | 1.12 | 0.014 | 0.007 | 0.017 | 0.041 | 0.063 |
| 120 | 0.00 | 2.92 | 1.66 | 1.43 | 1.66 | 0.015 | 0.007 | 0.019 | 0.046 | 0.094 |
| 180 | 0.00 | 3.34 | 1.46 | 1.99 | 1.46 | 0.014 | 0.006 | 0.017 | 0.078 | 0.108 |
| 240 | 0.00 | 3.22 | 1.70 | 1.21 | 1.70 | 0.013 | 0.006 | 0.016 | 0.025 | 0.118 |
| 300 | 0.00 | 3.32 | 1.13 | 1.87 | 1.13 | 0.012 | 0.005 | 0.015 | 0.117 | 0.131 |
| 360 | 0.00 | 3.03 | 1.63 | 1.71 | 1.63 | 0.011 | 0.005 | 0.015 | 0.045 | 0.117 |
| 420 | 0.00 | 3.30 | 1.93 | 1.44 | 1.93 | 0.010 | 0.005 | 0.014 | 0.007 | 0.123 |
| 480 | 0.00 | 3.21 | 1.48 | 2.33 | 1.48 | 0.009 | 0.004 | 0.014 | 0.109 | 0.124 |
| 540 | 0.00 | 3.52 | 1.48 | 2.14 | 1.48 | 0.010 | 0.004 | 0.014 | 0.107 | 0.154 |
| 720 | 0.00 | 4.09 | 3.26 | 3.02 | 3.26 | 0.011 | 0.005 | 0.014 | 0.133 | 0.183 |

**Table S3.** Time variation of **1**, [***Pd***Py*$_2$](BArF)$_2$, [***Pd***$_6$**1**$_3$](BArF)$_{12}$, Py*, and **Int**; ⟨*a*⟩–⟨*c*⟩ values of the average composition of the intermediates (***Pd***$_{\langle a\rangle}$**1**$_{\langle b\rangle}$Py*$_{\langle c\rangle}$); (⟨*n*⟩, ⟨*k*⟩) values for the self-assembly of [***Pd***$_6$**1**$_3$](BArF)$_{12}$ from **1** and [***Pd***Py*$_2$](BArF)$_2$ in $CD_3NO_2$ and $CDCl_3$ (2:1, v/v) at 298 K ([**1**]$_0$ = 0.5 mM) (run 1).

| Time / min | **1** / % | [***Pd***Py*$_2$](BArF)$_2$ / % | ***Pd***$_6$**1**$_3$ / % | Py* / % | **Int** / % | ⟨*a*⟩ | ⟨*b*⟩ | ⟨*c*⟩ | ⟨*n*⟩ | ⟨*k*⟩ |
|---|---|---|---|---|---|---|---|---|---|---|
| 0 | 100.0 | 100.0 | 0.0 | 0.0 | 0.0 | — | — | — | — | — |
| 5 | 0.0 | 47.2 | 0.0 | 34.5 | 100.0 | 0.119 | 0.110 | 0.083 | 1.417 | 1.085 |
| 10 | 0.0 | 42.4 | 3.5 | 39.7 | 96.5 | 0.122 | 0.106 | 0.081 | 1.546 | 1.154 |
| 15 | 0.0 | 38.2 | 4.7 | 43.4 | 95.3 | 0.129 | 0.105 | 0.083 | 1.674 | 1.234 |
| 20 | 0.0 | 36.6 | 5.6 | 44.9 | 94.4 | 0.131 | 0.104 | 0.083 | 1.719 | 1.261 |
| 25 | 0.0 | 34.0 | 7.8 | 47.4 | 92.2 | 0.132 | 0.101 | 0.084 | 1.776 | 1.302 |
| 30 | 0.0 | 32.8 | 9.0 | 49.3 | 91.0 | 0.132 | 0.100 | 0.081 | 1.830 | 1.321 |
| 35 | 0.0 | 32.6 | 10.8 | 50.1 | 89.2 | 0.128 | 0.098 | 0.078 | 1.823 | 1.312 |
| 40 | 0.0 | 31.7 | 11.1 | 51.9 | 88.9 | 0.130 | 0.098 | 0.074 | 1.899 | 1.329 |
| 45 | 0.0 | 31.0 | 12.2 | 53.3 | 87.8 | 0.129 | 0.096 | 0.071 | 1.939 | 1.338 |
| 50 | 0.0 | 31.6 | 13.7 | 52.1 | 86.3 | 0.124 | 0.095 | 0.074 | 1.846 | 1.312 |
| 55 | 0.0 | 31.3 | 14.0 | 52.9 | 86.0 | 0.124 | 0.094 | 0.071 | 1.879 | 1.318 |
| 60 | 0.0 | 30.9 | 15.6 | 53.4 | 84.4 | 0.122 | 0.093 | 0.071 | 1.860 | 1.313 |
| 120 | 0.0 | 28.0 | 24.5 | 56.8 | 75.5 | 0.109 | 0.083 | 0.069 | 1.795 | 1.312 |
| 180 | 0.0 | 26.9 | 31.5 | 59.7 | 68.5 | 0.096 | 0.075 | 0.060 | 1.742 | 1.273 |
| 240 | 0.0 | 26.1 | 35.4 | 61.6 | 64.6 | 0.089 | 0.071 | 0.055 | 1.733 | 1.256 |
| 300 | 0.0 | 25.8 | 42.3 | 63.0 | 57.7 | 0.075 | 0.063 | 0.051 | 1.558 | 1.178 |
| 360 | 0.0 | 25.5 | 43.6 | 63.1 | 56.4 | 0.072 | 0.062 | 0.051 | 1.509 | 1.170 |
| 420 | 0.0 | 25.2 | 46.5 | 64.5 | 53.5 | 0.067 | 0.059 | 0.047 | 1.478 | 1.135 |
| 480 | 0.0 | 25.2 | 49.7 | 64.1 | 50.3 | 0.060 | 0.055 | 0.048 | 1.282 | 1.079 |
| 540 | 0.0 | 24.5 | 52.3 | 64.7 | 47.7 | 0.056 | 0.052 | 0.049 | 1.194 | 1.063 |
| 720 | 0.0 | 23.5 | 54.2 | 65.6 | 45.8 | 0.054 | 0.050 | 0.049 | 1.154 | 1.066 |

**Table S4.** Time variation of **1**, [***Pd***Py*$_2$](BArF)$_2$, [***Pd***$_6$**1**$_3$](BArF)$_{12}$, Py*, and **Int**; ⟨*a*⟩–⟨*c*⟩ values of the average composition of the intermediates (***Pd***$_{\langle a\rangle}$**1**$_{\langle b\rangle}$Py*$_{\langle c\rangle}$); (⟨*n*⟩, ⟨*k*⟩) values for the self-assembly of [***Pd***$_6$**1**$_3$](BArF)$_{12}$ from **1** and [***Pd***Py*$_2$](BArF)$_2$ in $CD_3NO_2$ and $CDCl_3$ (2:1, v/v) at 298 K ([**1**]$_0$ = 0.5 mM) (run 2).

| Time / min | **1** / % | [***Pd***Py*$_2$](BArF)$_2$ / % | ***Pd***$_6$**1**$_3$ / % | Py* / % | **Int** / % | ⟨*a*⟩ | ⟨*b*⟩ | ⟨*c*⟩ | ⟨*n*⟩ | ⟨*k*⟩ |
|---|---|---|---|---|---|---|---|---|---|---|
| 0 | 100.0 | 100.0 | 0.0 | 0.0 | 0.0 | — | — | — | — | — |
| 5 | 0.0 | 57.7 | 1.3 | 37.2 | 98.7 | 0.072 | 0.083 | 0.018 | 1.514 | 0.863 |
| 10 | 0.0 | 53.6 | 2.3 | 40.9 | 97.7 | 0.078 | 0.083 | 0.019 | 1.644 | 0.939 |
| 15 | 0.0 | 51.2 | 5.4 | 44.1 | 94.6 | 0.077 | 0.080 | 0.017 | 1.709 | 0.957 |
| 20 | 0.0 | 48.0 | 6.6 | 46.3 | 93.4 | 0.080 | 0.079 | 0.020 | 1.777 | 1.016 |
| 25 | 0.0 | 45.5 | 8.3 | 48.4 | 91.7 | 0.082 | 0.077 | 0.022 | 1.829 | 1.053 |
| 30 | 0.0 | 44.1 | 10.2 | 49.8 | 89.8 | 0.081 | 0.076 | 0.021 | 1.848 | 1.065 |
| 35 | 0.0 | 43.4 | 11.7 | 51.4 | 88.3 | 0.080 | 0.075 | 0.018 | 1.888 | 1.066 |
| 40 | 0.0 | 41.8 | 12.7 | 52.4 | 87.3 | 0.081 | 0.074 | 0.020 | 1.913 | 1.095 |
| 45 | 0.0 | 41.3 | 14.7 | 54.2 | 85.3 | 0.078 | 0.072 | 0.016 | 1.953 | 1.085 |
| 50 | 0.0 | 40.5 | 15.6 | 54.5 | 84.4 | 0.078 | 0.071 | 0.018 | 1.944 | 1.096 |
| 55 | 0.0 | 40.0 | 17.5 | 55.9 | 82.5 | 0.076 | 0.070 | 0.014 | 1.966 | 1.086 |
| 60 | 0.0 | 39.1 | 18.2 | 56.4 | 81.8 | 0.076 | 0.069 | 0.016 | 1.973 | 1.101 |
| 120 | 0.0 | 37.0 | 30.0 | 61.6 | 70.0 | 0.060 | 0.059 | 0.005 | 1.942 | 1.011 |
| 180 | 0.0 | 36.5 | 36.2 | 63.2 | 63.8 | 0.050 | 0.054 | 0.001 | 1.848 | 0.933 |
| 240 | 0.0 | 35.9 | 41.0 | 64.4 | 59.0 | 0.043 | 0.050 | 0.000 | 1.733 | 0.866 |
| 300 | 0.0 | 35.8 | 46.2 | 67.5 | 53.8 | 0.035 | 0.045 | 0.000 | 1.519 | 0.759 |
| 360 | 0.0 | 34.0 | 48.1 | 67.4 | 51.9 | 0.035 | 0.044 | 0.000 | 1.579 | 0.790 |
| 420 | 0.0 | 34.4 | 49.9 | 68.5 | 50.1 | 0.031 | 0.042 | 0.000 | 1.456 | 0.728 |
| 480 | 0.0 | 33.6 | 52.6 | 69.5 | 47.4 | 0.028 | 0.040 | 0.000 | 1.379 | 0.690 |
| 540 | 0.0 | 33.8 | 55.8 | 69.8 | 44.2 | 0.022 | 0.037 | 0.000 | 1.166 | 0.583 |
| 720 | 0.0 | 33.7 | 59.5 | 69.7 | 40.5 | 0.016 | 0.034 | 0.000 | 0.919 | 0.459 |

**Table S5.** Time variation of **1**, [***Pd***Py*$_2$](BArF)$_2$, [***Pd***$_6$**1**$_3$](BArF)$_{12}$, Py*, and **Int**; ⟨*a*⟩–⟨*c*⟩ values of the average composition of the intermediates (***Pd***$_{\langle a\rangle}$**1**$_{\langle b\rangle}$Py*$_{\langle c\rangle}$); (⟨*n*⟩, ⟨*k*⟩) values for the self-assembly of [***Pd***$_6$**1**$_3$](BArF)$_{12}$ from **1** and [***Pd***Py*$_2$](BArF)$_2$ in $CD_3NO_2$ and $CDCl_3$ (2:1, v/v) at 298 K ([**1**]$_0$ = 0.5 mM) (run 3).

| Time / min | **1** / % | [***Pd***Py*$_2$](BArF)$_2$ / % | ***Pd***$_6$**1**$_3$ / % | Py* / % | **Int** / % | ⟨*a*⟩ | ⟨*b*⟩ | ⟨*c*⟩ | ⟨*n*⟩ | ⟨*k*⟩ |
|---|---|---|---|---|---|---|---|---|---|---|
| 0 | 100.0 | 100.0 | 0.0 | 0.0 | 0.0 | — | — | — | — | — |
| 5 | 0.0 | 50.2 | 0.0 | 35.8 | 100.0 | 0.104 | 0.103 | 0.059 | 1.458 | 1.016 |
| 10 | 0.0 | 45.0 | 2.6 | 38.4 | 97.4 | 0.109 | 0.100 | 0.069 | 1.500 | 1.097 |
| 15 | 0.0 | 42.2 | 4.1 | 41.3 | 95.9 | 0.112 | 0.098 | 0.069 | 1.585 | 1.143 |
| 20 | 0.0 | 39.8 | 5.8 | 45.7 | 94.2 | 0.114 | 0.097 | 0.061 | 1.730 | 1.179 |
| 25 | 0.0 | 38.9 | 7.2 | 46.0 | 92.8 | 0.113 | 0.095 | 0.063 | 1.712 | 1.187 |
| 30 | 0.0 | 36.8 | 8.2 | 47.7 | 91.8 | 0.115 | 0.094 | 0.065 | 1.759 | 1.225 |
| 35 | 0.0 | 35.9 | 9.7 | 49.1 | 90.3 | 0.114 | 0.093 | 0.063 | 1.784 | 1.231 |
| 40 | 0.0 | 35.4 | 11.2 | 49.4 | 88.8 | 0.112 | 0.091 | 0.063 | 1.765 | 1.230 |
| 45 | 0.0 | 34.7 | 12.0 | 50.9 | 88.0 | 0.112 | 0.090 | 0.060 | 1.814 | 1.239 |
| 50 | 0.0 | 33.5 | 13.0 | 50.9 | 87.0 | 0.112 | 0.089 | 0.066 | 1.785 | 1.260 |
| 55 | 0.0 | 33.0 | 14.6 | 52.7 | 85.4 | 0.110 | 0.088 | 0.060 | 1.834 | 1.259 |
| 60 | 0.0 | 33.3 | 14.4 | 52.8 | 85.6 | 0.110 | 0.088 | 0.058 | 1.842 | 1.253 |
| 120 | 0.0 | 28.5 | 25.8 | 60.3 | 74.2 | 0.097 | 0.076 | 0.047 | 1.921 | 1.268 |
| 180 | 0.0 | 26.1 | 35.5 | 66.6 | 64.5 | 0.082 | 0.066 | 0.031 | 2.010 | 1.236 |
| 240 | 0.0 | 26.4 | 39.8 | 65.7 | 60.2 | 0.072 | 0.062 | 0.033 | 1.808 | 1.169 |
| 300 | 0.0 | 25.9 | 44.4 | 69.3 | 55.6 | 0.064 | 0.057 | 0.020 | 1.887 | 1.121 |
| 360 | 0.0 | 24.4 | 48.8 | 68.8 | 51.2 | 0.058 | 0.053 | 0.028 | 1.666 | 1.103 |
| 420 | 0.0 | 23.9 | 53.2 | 69.1 | 46.8 | 0.050 | 0.048 | 0.029 | 1.476 | 1.040 |
| 480 | 0.0 | 23.1 | 54.8 | 72.0 | 45.2 | 0.048 | 0.046 | 0.020 | 1.647 | 1.043 |
| 540 | 0.0 | 22.3 | 57.3 | 71.9 | 42.7 | 0.045 | 0.044 | 0.024 | 1.501 | 1.023 |
| 720 | 0.0 | 20.1 | 65.5 | 76.0 | 34.5 | 0.033 | 0.035 | 0.016 | 1.381 | 0.920 |

Time variation of **2**, [***Pd***Py*$_2$](BF$_4$)$_2$, [***Pd***$_6$**2**$_3$](BF$_4$)$_{12}$, Py*, **Int**, and the (⟨*n*⟩, ⟨*k*⟩) values for the self-assembly of the [***Pd***$_6$**2**$_3$](BF$_4$)$_{12}$ prism (Tables S6–S10)

**Table S6.** Average time variation of **2**, [***Pd***Py*$_2$](BF$_4$)$_2$, [***Pd***$_6$**2**$_3$](BF$_4$)$_{12}$, Py*, and **Int**; ⟨*a*⟩–⟨*c*⟩ values of the average composition of the intermediates (Pd$_{\langle a\rangle}$**2**$_{\langle b\rangle}$Py*$_{\langle c\rangle}$); (⟨*n*⟩, ⟨*k*⟩) values for the self-assembly of [***Pd***$_6$**2**$_3$](BF$_4$)$_{12}$ from **2** and [***Pd***Py*$_2$](BF$_4$)$_2$ in CD$_3$NO$_2$ and CDCl$_3$ (4:1, v/v) ([**2**]$_0$ = *ca* 1.0 mM).

| Time / min | **2** / % | [***Pd***Py*$_2$](BF$_4$)$_2$ / % | ***Pd***$_6$**2**$_3$ / % | Py* / % | **Int** / % | ⟨*a*⟩ | ⟨*b*⟩ | ⟨*c*⟩ | ⟨*n*⟩ | ⟨*k*⟩ |
|---|---|---|---|---|---|---|---|---|---|---|
| 0 | 100.0 | 100.0 | 0.0 | 0.0 | 0.0 | — | — | — | — | — |
| 5 | 9.3 | 74.4 | 0.0 | 20.4 | 90.7 | 0.098 | 0.173 | 0.040 | 0.905 | 0.569 |
| 10 | 3.6 | 60.6 | 0.0 | 29.4 | 96.4 | 0.152 | 0.184 | 0.077 | 1.229 | 0.825 |
| 15 | 0.0 | 50.9 | 0.0 | 35.8 | 100.0 | 0.189 | 0.191 | 0.103 | 1.445 | 0.992 |
| 20 | 0.0 | 44.6 | 0.0 | 40.5 | 100.0 | 0.213 | 0.191 | 0.115 | 1.635 | 1.118 |
| 25 | 0.0 | 40.5 | 0.0 | 43.8 | 100.0 | 0.229 | 0.191 | 0.121 | 1.767 | 1.201 |
| 30 | 0.0 | 38.8 | 0.0 | 47.1 | 100.0 | 0.236 | 0.191 | 0.109 | 1.902 | 1.236 |
| 35 | 0.0 | 36.4 | 0.0 | 49.2 | 100.0 | 0.245 | 0.191 | 0.111 | 1.985 | 1.284 |
| 40 | 0.0 | 33.5 | 0.0 | 50.2 | 100.0 | 0.256 | 0.191 | 0.126 | 2.027 | 1.342 |
| 45 | 0.0 | 32.0 | 0.0 | 51.8 | 100.0 | 0.262 | 0.191 | 0.125 | 2.094 | 1.374 |
| 50 | 0.0 | 30.8 | 0.0 | 53.4 | 100.0 | 0.266 | 0.191 | 0.122 | 2.155 | 1.397 |
| 55 | 0.0 | 29.7 | 0.0 | 53.5 | 100.0 | 0.271 | 0.191 | 0.129 | 2.161 | 1.419 |
| 60 | 0.0 | 29.6 | 0.0 | 55.3 | 100.0 | 0.271 | 0.191 | 0.117 | 2.234 | 1.422 |
| 120 | 0.0 | 24.3 | 0.0 | 61.6 | 100.0 | 0.292 | 0.191 | 0.109 | 2.488 | 1.529 |
| 180 | 0.0 | 22.0 | 0.0 | 63.7 | 100.0 | 0.300 | 0.191 | 0.110 | 2.571 | 1.574 |
| 240 | 0.0 | 21.6 | 0.0 | 65.6 | 100.0 | 0.302 | 0.191 | 0.098 | 2.651 | 1.582 |
| 300 | 0.0 | 21.6 | 0.0 | 66.6 | 100.0 | 0.302 | 0.191 | 0.091 | 2.690 | 1.584 |
| 360 | 0.0 | 20.5 | 0.0 | 67.4 | 100.0 | 0.306 | 0.191 | 0.093 | 2.722 | 1.606 |
| 720 | 0.0 | 19.5 | 3.0 | 72.5 | 97.0 | 0.299 | 0.185 | 0.061 | 2.893 | 1.612 |
| 1440 | 0.0 | 17.5 | 9.8 | 76.4 | 90.2 | 0.281 | 0.172 | 0.048 | 2.985 | 1.628 |
| 2160 | 0.0 | 16.2 | 16.4 | 79.1 | 83.6 | 0.261 | 0.160 | 0.037 | 3.035 | 1.629 |
| 2220 | 0.0 | 12.7 | 27.6 | 83.1 | 72.4 | 0.231 | 0.138 | 0.033 | 3.114 | 1.669 |
| 2280 | 0.0 | 11.1 | 33.6 | 84.8 | 66.4 | 0.215 | 0.127 | 0.032 | 3.140 | 1.686 |
| 2400 | 0.0 | 9.0 | 44.2 | 86.8 | 55.8 | 0.182 | 0.107 | 0.033 | 3.116 | 1.703 |
| 2520 | 0.0 | 8.6 | 49.7 | 88.8 | 50.3 | 0.163 | 0.096 | 0.020 | 3.177 | 1.688 |
| 2880 | 0.0 | 6.4 | 59.9 | 90.1 | 40.1 | 0.132 | 0.076 | 0.027 | 3.103 | 1.718 |
| 3600 | 0.0 | 4.8 | 68.4 | 92.4 | 31.6 | 0.106 | 0.060 | 0.021 | 3.162 | 1.743 |
| 5040 | 0.0 | 3.5 | 74.7 | 93.9 | 25.3 | 0.087 | 0.048 | 0.024 | 3.147 | 1.793 |
| 6480 | 0.0 | 3.2 | 75.2 | 93.6 | 24.8 | 0.086 | 0.047 | 0.025 | 3.134 | 1.817 |

**Table S7.** Standard errors for each time point of **2**, [***Pd***Py*$_2$](BF$_4$)$_2$, [***Pd***$_6$**2**$_3$](BF$_4$)$_{12}$, Py*, and **Int**; ⟨*a*⟩–⟨*c*⟩ values of the average composition of the intermediates (Pd$_{\langle a\rangle}$**2**$_{\langle b\rangle}$Py*$_{\langle c\rangle}$); (⟨*n*⟩, ⟨*k*⟩) values for the self-assembly of [***Pd***$_6$**2**$_3$](BF$_4$)$_{12}$ from **2** and [***Pd***Py*$_2$](BF$_4$)$_2$ in CD$_3$NO$_2$ and CDCl$_3$ (4:1, v/v) ([**2**]$_0$ = *ca* 1.0 mM).

| Time / min | **2** / % | [***Pd***Py*$_2$](BF$_4$)$_2$ / % | ***Pd***$_6$**2**$_3$ / % | Py* / % | **Int** / % | ⟨*a*⟩ | ⟨*b*⟩ | ⟨*c*⟩ | ⟨*n*⟩ | ⟨*k*⟩ |
|---|---|---|---|---|---|---|---|---|---|---|
| 0 | 0.00 | 0.00 | 0.00 | 0.00 | 0.00 | — | — | — | — | — |
| 5 | 2.55 | 2.30 | 0.00 | 1.45 | 2.55 | 0.008 | 0.005 | 0.006 | 0.051 | 0.043 |
| 10 | 1.81 | 2.01 | 0.00 | 1.78 | 1.81 | 0.006 | 0.003 | 0.001 | 0.061 | 0.036 |
| 15 | 0.00 | 2.17 | 0.00 | 1.42 | 0.00 | 0.007 | 0.001 | 0.008 | 0.045 | 0.041 |
| 20 | 0.00 | 1.05 | 0.00 | 1.48 | 0.00 | 0.002 | 0.001 | 0.005 | 0.049 | 0.017 |
| 25 | 0.00 | 1.44 | 0.00 | 1.63 | 0.00 | 0.003 | 0.001 | 0.004 | 0.058 | 0.020 |
| 30 | 0.00 | 1.09 | 0.00 | 1.82 | 0.00 | 0.004 | 0.001 | 0.009 | 0.058 | 0.023 |
| 35 | 0.00 | 1.34 | 0.00 | 1.30 | 0.00 | 0.002 | 0.001 | 0.004 | 0.041 | 0.013 |
| 40 | 0.00 | 1.30 | 0.00 | 1.45 | 0.00 | 0.002 | 0.001 | 0.011 | 0.052 | 0.007 |
| 45 | 0.00 | 0.75 | 0.00 | 1.33 | 0.00 | 0.003 | 0.001 | 0.007 | 0.036 | 0.017 |
| 50 | 0.00 | 1.18 | 0.00 | 1.64 | 0.00 | 0.001 | 0.001 | 0.011 | 0.057 | 0.004 |
| 55 | 0.00 | 0.67 | 0.00 | 2.02 | 0.00 | 0.004 | 0.001 | 0.018 | 0.065 | 0.013 |
| 60 | 0.00 | 0.55 | 0.00 | 1.50 | 0.00 | 0.004 | 0.001 | 0.013 | 0.043 | 0.013 |
| 120 | 0.00 | 0.70 | 0.00 | 1.01 | 0.00 | 0.003 | 0.001 | 0.007 | 0.021 | 0.009 |
| 180 | 0.00 | 1.05 | 0.00 | 1.07 | 0.00 | 0.003 | 0.001 | 0.006 | 0.015 | 0.008 |
| 240 | 0.00 | 1.18 | 0.00 | 1.07 | 0.00 | 0.004 | 0.001 | 0.009 | 0.020 | 0.012 |
| 300 | 0.00 | 1.07 | 0.00 | 1.39 | 0.00 | 0.006 | 0.001 | 0.016 | 0.042 | 0.020 |
| 360 | 0.00 | 1.37 | 0.00 | 1.15 | 0.00 | 0.005 | 0.001 | 0.013 | 0.033 | 0.016 |
| 720 | 0.00 | 1.51 | 1.57 | 1.10 | 1.57 | 0.011 | 0.004 | 0.011 | 0.008 | 0.025 |
| 1440 | 0.00 | 1.70 | 2.55 | 1.79 | 2.55 | 0.014 | 0.006 | 0.014 | 0.023 | 0.030 |
| 2160 | 0.00 | 1.53 | 3.92 | 1.78 | 3.92 | 0.019 | 0.008 | 0.015 | 0.020 | 0.033 |
| 2220 | 0.00 | 1.21 | 4.46 | 2.22 | 4.46 | 0.021 | 0.009 | 0.019 | 0.044 | 0.037 |
| 2280 | 0.00 | 1.47 | 4.30 | 2.01 | 4.30 | 0.020 | 0.009 | 0.018 | 0.053 | 0.039 |
| 2400 | 0.00 | 1.16 | 3.89 | 1.31 | 3.89 | 0.018 | 0.008 | 0.014 | 0.088 | 0.037 |
| 2520 | 0.00 | 1.10 | 3.59 | 1.16 | 3.59 | 0.016 | 0.007 | 0.011 | 0.062 | 0.042 |
| 2880 | 0.00 | 1.04 | 2.72 | 0.92 | 2.72 | 0.013 | 0.006 | 0.010 | 0.097 | 0.046 |
| 3600 | 0.00 | 0.90 | 2.41 | 1.22 | 2.41 | 0.012 | 0.005 | 0.011 | 0.138 | 0.054 |
| 5040 | 0.00 | 0.72 | 2.83 | 2.00 | 2.83 | 0.011 | 0.006 | 0.016 | 0.183 | 0.072 |
| 6480 | 0.00 | 0.77 | 1.22 | 2.35 | 1.22 | 0.007 | 0.003 | 0.021 | 0.250 | 0.088 |

**Table S8.** Time variation of **2**, [***Pd***Py*$_2$](BF$_4$)$_2$, [***Pd***$_6$**2**$_3$](BF$_4$)$_{12}$, Py*, and **Int**; ⟨*a*⟩–⟨*c*⟩ values of the average composition of the intermediates (***Pd***$_{\langle a\rangle}$**2**$_{\langle b\rangle}$Py*$_{\langle c\rangle}$); (⟨*n*⟩, ⟨*k*⟩) values for the self-assembly of [***Pd***$_6$**2**$_3$](BF$_4$)$_{12}$ from **2** and [***Pd***Py*$_2$](BF$_4$)$_2$ in $CD_3NO_2$ and $CDCl_3$ (4:1, v/v) ([**2**]$_0$ = 1.0 mM) (run 1).

| Time / min | **2** / % | [***Pd***Py*$_2$](BF$_4$)$_2$ / % | ***Pd***$_6$**2**$_3$ / % | Py* / % | **Int** / % | ⟨*a*⟩ | ⟨*b*⟩ | ⟨*c*⟩ | ⟨*n*⟩ | ⟨*k*⟩ |
|---|---|---|---|---|---|---|---|---|---|---|
| 0 | 100.0 | 100.0 | 0.0 | 0.0 | 0.0 | — | — | — | — | — |
| 5 | 4.2 | 71.7 | 0.0 | 22.2 | 95.8 | 0.106 | 0.182 | 0.046 | 0.909 | 0.581 |
| 10 | 0.0 | 57.9 | 0.0 | 31.8 | 100.0 | 0.157 | 0.190 | 0.077 | 1.248 | 0.827 |
| 15 | 0.0 | 49.0 | 0.0 | 37.9 | 100.0 | 0.190 | 0.190 | 0.098 | 1.488 | 1.000 |
| 20 | 0.0 | 43.3 | 0.0 | 42.5 | 100.0 | 0.212 | 0.190 | 0.106 | 1.669 | 1.113 |
| 25 | 0.0 | 38.3 | 0.0 | 45.5 | 100.0 | 0.230 | 0.190 | 0.121 | 1.785 | 1.211 |
| 30 | 0.0 | 38.0 | 0.0 | 49.7 | 100.0 | 0.232 | 0.190 | 0.092 | 1.951 | 1.217 |
| 35 | 0.0 | 33.9 | 0.0 | 50.8 | 100.0 | 0.247 | 0.190 | 0.114 | 1.993 | 1.297 |
| 40 | 0.0 | 30.9 | 0.0 | 51.7 | 100.0 | 0.258 | 0.190 | 0.130 | 2.029 | 1.356 |
| 45 | 0.0 | 31.2 | 0.0 | 54.0 | 100.0 | 0.257 | 0.190 | 0.111 | 2.121 | 1.351 |
| 50 | 0.0 | 28.4 | 0.0 | 55.2 | 100.0 | 0.267 | 0.190 | 0.123 | 2.167 | 1.405 |
| 55 | 0.0 | 28.7 | 0.0 | 56.3 | 100.0 | 0.266 | 0.190 | 0.112 | 2.210 | 1.400 |
| 60 | 0.0 | 28.7 | 0.0 | 57.6 | 100.0 | 0.266 | 0.190 | 0.102 | 2.262 | 1.400 |
| 120 | 0.0 | 22.9 | 0.0 | 63.4 | 100.0 | 0.288 | 0.190 | 0.102 | 2.490 | 1.513 |
| 180 | 0.0 | 20.1 | 0.0 | 65.7 | 100.0 | 0.298 | 0.190 | 0.106 | 2.581 | 1.568 |
| 240 | 0.0 | 19.6 | 0.0 | 67.6 | 100.0 | 0.301 | 0.190 | 0.096 | 2.656 | 1.579 |
| 300 | 0.0 | 20.4 | 0.0 | 68.5 | 100.0 | 0.297 | 0.190 | 0.083 | 2.690 | 1.563 |
| 360 | 0.0 | 18.3 | 0.0 | 69.1 | 100.0 | 0.305 | 0.190 | 0.094 | 2.715 | 1.605 |
| 720 | 0.0 | 17.1 | 3.7 | 74.4 | 96.3 | 0.295 | 0.183 | 0.063 | 2.880 | 1.612 |
| 1440 | 0.0 | 14.5 | 10.1 | 79.5 | 89.9 | 0.281 | 0.171 | 0.045 | 3.023 | 1.642 |
| 2160 | 0.0 | 13.4 | 17.7 | 81.5 | 82.3 | 0.256 | 0.157 | 0.038 | 3.029 | 1.636 |
| 2220 | 0.0 | 10.6 | 28.8 | 85.9 | 71.2 | 0.224 | 0.135 | 0.026 | 3.116 | 1.655 |
| 2280 | 0.0 | 8.5 | 36.2 | 87.2 | 63.8 | 0.204 | 0.121 | 0.032 | 3.099 | 1.679 |
| 2400 | 0.0 | 6.9 | 47.1 | 87.8 | 52.9 | 0.169 | 0.101 | 0.040 | 2.958 | 1.675 |
| 2520 | 0.0 | 6.6 | 51.8 | 90.3 | 48.2 | 0.152 | 0.092 | 0.023 | 3.061 | 1.655 |
| 2880 | 0.0 | 4.6 | 61.1 | 91.2 | 38.9 | 0.124 | 0.074 | 0.032 | 2.916 | 1.674 |
| 3600 | 0.0 | 3.2 | 70.1 | 93.8 | 29.9 | 0.095 | 0.057 | 0.022 | 2.939 | 1.664 |
| 5040 | 0.0 | 2.5 | 71.2 | 95.3 | 28.8 | 0.093 | 0.055 | 0.017 | 3.105 | 1.703 |
| 6480 | 0.0 | 2.3 | 74.0 | 97.0 | 26.0 | 0.083 | 0.049 | 0.005 | 3.256 | 1.681 |

**Table S9.** Time variation of **2**, [***Pd***Py*$_2$](BF$_4$)$_2$, [***Pd***$_6$**2**$_3$](BF$_4$)$_{12}$, Py*, and **Int**; ⟨*a*⟩–⟨*c*⟩ values of the average composition of the intermediates (***Pd***$_{\langle a\rangle}$**2**$_{\langle b\rangle}$Py*$_{\langle c\rangle}$); (⟨*n*⟩, ⟨*k*⟩) values for the self-assembly of [***Pd***$_6$**2**$_3$](BF$_4$)$_{12}$ from **2** and [***Pd***Py*$_2$](BF$_4$)$_2$ in $CD_3NO_2$ and $CDCl_3$ (4:1, v/v) ([**2**]$_0$ = 1.0 mM) (run 2).

| Time / min | **2** / % | [***Pd***Py*$_2$](BF$_4$)$_2$ / % | ***Pd***$_6$**2**$_3$ / % | Py* / % | **Int** / % | ⟨*a*⟩ | ⟨*b*⟩ | ⟨*c*⟩ | ⟨*n*⟩ | ⟨*k*⟩ |
|---|---|---|---|---|---|---|---|---|---|---|
| 0 | 100.0 | 100.0 | 0.0 | 0.0 | 0.0 | — | — | — | — | — |
| 5 | 11.7 | 72.6 | 0.0 | 21.4 | 88.3 | 0.106 | 0.167 | 0.047 | 0.992 | 0.636 |
| 10 | 5.9 | 59.3 | 0.0 | 30.4 | 94.1 | 0.158 | 0.178 | 0.080 | 1.324 | 0.886 |
| 15 | 0.0 | 48.4 | 0.0 | 36.4 | 100.0 | 0.200 | 0.190 | 0.118 | 1.493 | 1.058 |
| 20 | 0.0 | 43.9 | 0.0 | 41.4 | 100.0 | 0.218 | 0.190 | 0.114 | 1.699 | 1.150 |
| 25 | 0.0 | 40.0 | 0.0 | 45.3 | 100.0 | 0.233 | 0.190 | 0.114 | 1.857 | 1.229 |
| 30 | 0.0 | 37.5 | 0.0 | 48.0 | 100.0 | 0.243 | 0.190 | 0.113 | 1.968 | 1.282 |
| 35 | 0.0 | 36.7 | 0.0 | 50.1 | 100.0 | 0.246 | 0.190 | 0.103 | 2.052 | 1.298 |
| 40 | 0.0 | 34.9 | 0.0 | 51.6 | 100.0 | 0.253 | 0.190 | 0.105 | 2.116 | 1.334 |
| 45 | 0.0 | 31.3 | 0.0 | 52.1 | 100.0 | 0.267 | 0.190 | 0.129 | 2.137 | 1.408 |
| 50 | 0.0 | 31.9 | 0.0 | 54.8 | 100.0 | 0.264 | 0.190 | 0.103 | 2.247 | 1.395 |
| 55 | 0.0 | 31.0 | 0.0 | 54.7 | 100.0 | 0.268 | 0.190 | 0.111 | 2.242 | 1.414 |
| 60 | 0.0 | 30.6 | 0.0 | 55.9 | 100.0 | 0.269 | 0.190 | 0.105 | 2.290 | 1.422 |
| 120 | 0.0 | 25.2 | 0.0 | 61.6 | 100.0 | 0.291 | 0.190 | 0.103 | 2.524 | 1.533 |
| 180 | 0.0 | 23.7 | 0.0 | 63.2 | 100.0 | 0.296 | 0.190 | 0.102 | 2.590 | 1.563 |
| 240 | 0.0 | 23.7 | 0.0 | 65.4 | 100.0 | 0.296 | 0.190 | 0.084 | 2.682 | 1.563 |
| 300 | 0.0 | 23.7 | 0.0 | 67.4 | 100.0 | 0.296 | 0.190 | 0.069 | 2.763 | 1.564 |
| 360 | 0.0 | 23.0 | 0.0 | 67.9 | 100.0 | 0.299 | 0.190 | 0.071 | 2.782 | 1.579 |
| 720 | 0.0 | 22.3 | 5.3 | 72.4 | 94.7 | 0.282 | 0.180 | 0.041 | 2.908 | 1.569 |
| 1440 | 0.0 | 20.4 | 14.0 | 76.3 | 86.0 | 0.256 | 0.163 | 0.025 | 2.987 | 1.570 |
| 2160 | 0.0 | 18.7 | 22.5 | 80.1 | 77.5 | 0.231 | 0.147 | 0.010 | 3.072 | 1.570 |
| 2220 | 0.0 | 14.8 | 34.6 | 84.6 | 65.4 | 0.200 | 0.124 | 0.005 | 3.189 | 1.613 |
| 2280 | 0.0 | 13.6 | 39.4 | 86.4 | 60.6 | 0.187 | 0.115 | 0.000 | 3.244 | 1.623 |
| 2400 | 0.0 | 10.9 | 49.0 | 88.4 | 51.0 | 0.160 | 0.097 | 0.006 | 3.262 | 1.659 |
| 2520 | 0.0 | 10.4 | 54.6 | 89.5 | 45.4 | 0.141 | 0.086 | 0.000 | 3.271 | 1.638 |
| 2880 | 0.0 | 8.2 | 63.9 | 90.9 | 36.1 | 0.114 | 0.068 | 0.007 | 3.243 | 1.670 |
| 3600 | 0.0 | 6.3 | 71.4 | 93.5 | 28.6 | 0.093 | 0.054 | 0.001 | 3.415 | 1.718 |
| 5040 | 0.0 | 4.9 | 80.3 | 96.5 | 19.7 | 0.065 | 0.037 | 0.000 | 3.482 | 1.741 |
| 6480 | 0.0 | 4.7 | 77.6 | 94.8 | 22.4 | 0.076 | 0.042 | 0.003 | 3.493 | 1.787 |

**Table S10.** Time variation of **2**, [***Pd***Py*$_2$](BF$_4$)$_2$, [***Pd***$_6$**2**$_3$](BF$_4$)$_{12}$, Py*, and **Int**; ⟨*a*⟩–⟨*c*⟩ values of the average composition of the intermediates (***Pd***$_{\langle a\rangle}$**2**$_{\langle b\rangle}$Py*$_{\langle c\rangle}$); (⟨*n*⟩, ⟨*k*⟩) values for the self-assembly of [***Pd***$_6$**2**$_3$](BF$_4$)$_{12}$ from **2** and [***Pd***Py*$_2$](BF$_4$)$_2$ in $CD_3NO_2$ and $CDCl_3$ (4:1, v/v) ([**2**]$_0$ = 1.0 mM) (run 3).

| Time / min | **2** / % | [***Pd***Py*$_2$](BF$_4$)$_2$ / % | ***Pd***$_6$**2**$_3$ / % | Py* / % | **Int** / % | ⟨*a*⟩ | ⟨*b*⟩ | ⟨*c*⟩ | ⟨*n*⟩ | ⟨*k*⟩ |
|---|---|---|---|---|---|---|---|---|---|---|
| 0 | 100.0 | 100.0 | 0.0 | 0.0 | 0.0 | — | — | — | — | — |
| 5 | 12.0 | 79.0 | 0.0 | 17.5 | 88.0 | 0.083 | 0.170 | 0.028 | 0.815 | 0.489 |
| 10 | 4.8 | 64.5 | 0.0 | 25.9 | 95.2 | 0.140 | 0.183 | 0.075 | 1.116 | 0.762 |
| 15 | 0.0 | 55.2 | 0.0 | 33.1 | 100.0 | 0.177 | 0.193 | 0.093 | 1.355 | 0.918 |
| 20 | 0.0 | 46.7 | 0.0 | 37.6 | 100.0 | 0.210 | 0.193 | 0.124 | 1.538 | 1.091 |
| 25 | 0.0 | 43.2 | 0.0 | 40.5 | 100.0 | 0.224 | 0.193 | 0.128 | 1.658 | 1.162 |
| 30 | 0.0 | 41.0 | 0.0 | 43.6 | 100.0 | 0.233 | 0.193 | 0.121 | 1.787 | 1.208 |
| 35 | 0.0 | 38.5 | 0.0 | 46.6 | 100.0 | 0.242 | 0.193 | 0.117 | 1.910 | 1.258 |
| 40 | 0.0 | 34.7 | 0.0 | 47.3 | 100.0 | 0.258 | 0.193 | 0.142 | 1.937 | 1.337 |
| 45 | 0.0 | 33.5 | 0.0 | 49.4 | 100.0 | 0.262 | 0.193 | 0.135 | 2.023 | 1.362 |
| 50 | 0.0 | 32.0 | 0.0 | 50.1 | 100.0 | 0.268 | 0.193 | 0.141 | 2.050 | 1.392 |
| 55 | 0.0 | 29.5 | 0.0 | 49.6 | 100.0 | 0.278 | 0.193 | 0.165 | 2.032 | 1.444 |
| 60 | 0.0 | 29.4 | 0.0 | 52.5 | 100.0 | 0.278 | 0.193 | 0.143 | 2.149 | 1.445 |
| 120 | 0.0 | 24.7 | 0.0 | 59.9 | 100.0 | 0.297 | 0.193 | 0.122 | 2.451 | 1.542 |
| 180 | 0.0 | 22.3 | 0.0 | 62.1 | 100.0 | 0.306 | 0.193 | 0.123 | 2.542 | 1.590 |
| 240 | 0.0 | 21.6 | 0.0 | 63.9 | 100.0 | 0.309 | 0.193 | 0.115 | 2.615 | 1.605 |
| 300 | 0.0 | 20.6 | 0.0 | 63.9 | 100.0 | 0.313 | 0.193 | 0.122 | 2.616 | 1.624 |
| 360 | 0.0 | 20.2 | 0.0 | 65.2 | 100.0 | 0.315 | 0.193 | 0.115 | 2.668 | 1.633 |
| 720 | 0.0 | 19.2 | 0.0 | 70.6 | 100.0 | 0.319 | 0.193 | 0.080 | 2.892 | 1.654 |
| 1440 | 0.0 | 17.5 | 5.2 | 73.3 | 94.8 | 0.305 | 0.183 | 0.073 | 2.945 | 1.671 |
| 2160 | 0.0 | 16.4 | 9.1 | 75.6 | 90.9 | 0.295 | 0.175 | 0.063 | 3.005 | 1.682 |
| 2220 | 0.0 | 12.6 | 19.3 | 78.7 | 80.7 | 0.270 | 0.155 | 0.068 | 3.038 | 1.739 |
| 2280 | 0.0 | 11.2 | 25.2 | 80.8 | 74.8 | 0.253 | 0.144 | 0.063 | 3.076 | 1.756 |
| 2400 | 0.0 | 9.2 | 36.5 | 84.2 | 63.5 | 0.217 | 0.122 | 0.052 | 3.129 | 1.776 |
| 2520 | 0.0 | 8.7 | 42.7 | 86.5 | 57.3 | 0.195 | 0.110 | 0.038 | 3.198 | 1.771 |
| 2880 | 0.0 | 6.5 | 54.7 | 88.3 | 45.3 | 0.158 | 0.087 | 0.041 | 3.151 | 1.811 |
| 3600 | 0.0 | 5.0 | 63.6 | 90.0 | 36.4 | 0.129 | 0.070 | 0.039 | 3.132 | 1.846 |
| 5040 | 0.0 | 3.1 | 72.6 | 90.0 | 27.4 | 0.102 | 0.053 | 0.054 | 2.853 | 1.936 |
| 6480 | 0.0 | 2.5 | 73.9 | 89.1 | 26.1 | 0.100 | 0.050 | 0.066 | 2.652 | 1.982 |

## NASAP (numerical analysis of self-assembly process) by a network model

For the numerical analysis of self-assembly process (NASAP), a reaction network for the self-assembly of the $[\boldsymbol{Pd}_6L_3]^{12+}$ prism, which is indicated as (6,3,0), is constructed as follows. Starting from the final prism (6,3,0), the reaction path is traced back to the substrates, that is, $[\boldsymbol{Pd}Py^*_2]^{2+}$ and L. In this back propagation process, all the directly accessible molecular species are considered as the intermediates. Note that for the compositions (4,3,0), (5,3,1), and (6,3,2), possible *trans*-isomers were also considered in the network. With these procedures taken, it is found that the total of 168 molecular species (including both the substrates and the product themselves) construct a minimal reaction network composed of 955 reactions, each of which contains the forward and backward processes. All the intermediates considered in this network model and a simplified reaction network are shown in Figure S8.

Although we call it as minimal, this reaction network turns out to be so large that it is impossible to assign individual rate constant to each reaction and to search for the parameter in such a vast parameter space to fit the experimental results best. Therefore, we divided the whole elementary reactions into seven classes possessing similar characteristics and defined rate constants as follows (Figure 3):

1. For the coordination of a free tetratopic ligand L releasing a leaving ligand X: $k_1$ [min$^{-1}$ M$^{-1}$] and $k_{-1}$ [min$^{-1}$ M$^{-1}$] for forward and backward reactions, respectively.
2. For the coordination bond of the Pd(II) and the ligand L at the second site of L, which is already coordinated by another Pd(II): $k_2$ [min$^{-1}$ M$^{-1}$] and $k_{-2}$ [min$^{-1}$ M$^{-1}$] for forward and backward reactions, respectively.
3. For the coordination bond of the Pd(II) and the ligand L at the third site of L, which is already coordinated by other two Pd(II)s: $k_3$ [min$^{-1}$ M$^{-1}$] and $k_{-3}$ [min$^{-1}$ M$^{-1}$] for forward and backward reactions, respectively.
4. For the coordination bond of the Pd(II) and the ligand L at the fourth (final) site of L: $k_4$ [min$^{-1}$ M$^{-1}$] and $k_{-4}$ [min$^{-1}$ M$^{-1}$] for forward and backward reactions, respectively.
5. For the intramolecular bridging in linear (non-cycle) species: $k_5$ [min$^{-1}$] and $k_{-5}$ [min$^{-1}$ M$^{-1}$] for forward and backward reactions, respectively.
6. For the intramolecular bridging in cyclized species: $k_6$ [min$^{-1}$] and $k_{-6}$ [min$^{-1}$ M$^{-1}$] for forward and backward reactions, respectively.
7. For the cyclization reaction: $k_7$ [min$^{-1}$] and $k_{-7}$ [min$^{-1}$ M$^{-1}$] for forward and backward reactions, respectively.

Note here that each rate constant is defined per reaction site, based on the above modeling procedure. So the actual reaction rate for each reaction is estimated as the defined constant multiplied by the total number of available combinations. For example, for a ligand reaction between $MX_2$ and a tetratopic ligand L to produce MLX and X, the rate constant is given as $k_1$ times 2 (the number of M–X bonds in $MX_2$) times 4 (the number of coordination sites in L), i.e.,

$$\mathrm{MX_2 + L} \xrightarrow{8k_1} \mathrm{MLX + X}.$$

We adopted this setting to explicitly distinguish the structural difference among the species with the same composition.

In order to numerically track the time evolution of the existence ratios for both reactants and products and the ($\langle n \rangle$, $\langle k \rangle$) values determined by QASAP, we have adopted a stochastic approach based on the chemical master equation, the so-called Gillespie algorithm. In this algorithm, for all the possible $N$ reactions including molecular species $S_{ai}$, $S_{bi}$, $S_{ci}$, …,

$$S_{ai} + S_{bi} + \ldots \rightarrow S_{ci} + \ldots \quad (i = 1, \ldots, N),$$

The total reaction rate $R_{tot}$ is calculated as

$$R_{tot} = r_1 + r_2 + \cdots + r_N,$$

$$r_i = k_i[S_{ai}][S_{bi}] \ldots.$$

Starting from the initial time $t = 0$, at each instant $t$, which one of the reactions to occur is determined with the uniform random number, $s_1 \in (0,1)$ as

$$\text{if } s_1 \leq \frac{r_1}{R_{tot}}, \text{ then reaction 1 occurs,}$$

$$\text{if } \frac{r_1}{R_{tot}} < s_1 \leq \frac{r_1+r_2}{R_{tot}} \text{ , then reaction 2 occurs,}$$

$$\text{if } \frac{r_1+\cdots+r_{N-1}}{R_{tot}} < s_1 \leq 1, \text{ then reaction } N \text{ occurs.}$$

Another uniform random number $s_2 \in (0,1)$ is independently given to fix the incremental $dt$ as

$$dt = \ln(1/s_2)/R_{tot}.$$

Time is updated as $t = t + dt$, together with the update of the numbers of corresponding molecular species, i.e., $\langle S_{ai}\rangle \to \langle S_{ai}\rangle - 1$, $\langle S_{bi}\rangle \to \langle S_{bi}\rangle - 1$, $\langle S_{ci}\rangle \to \langle S_{ci}\rangle + 1$, …. The reason why this approach traces the chemical reactions and actually works well is given in the literatures in detail, along with the practical way to implement it[8]. And for the NASAP applied to other coordination self-assembly systems, see literatures in reference 9.

For the ligand **1**, with the initial conditions (numbers of species), $\langle[\boldsymbol{Pd}\text{Py*}_2]^{2+}\rangle_0$ = 2,400, $\langle\mathbf{1}\rangle_0$ = 1,200, $\langle\text{others}\rangle_0$ = 0, rate constant search was performed in a fourteen-dimensional parameter space ($k_1$, $k_{-1}$, $k_2$, $k_{-2}$, $k_3$, $k_{-3}$, $k_4$, $k_{-4}$, $k_5$, $k_{-5}$, $k_6$, $k_{-6}$, $k_7$, $k_{-7}$). The Avogadro number and the volume of the simulation box were set to be $N_A = 6.0 \times 10^{23}$ and $V = 5.0 \times 10^{-18}$ L, respectively, which give the same concentrations as the experiments were carried out under. After the rate constant search was finished, refined simulations were performed for some rate parameter sets that give existence ratios and the *n–k* plot in good agreement with the experimental counterparts.

The program for fitting the rate constant values is handmade for only this purpose. In order to obtain one of the best constant sets, the following practical procedures are taken:

1. First, the rate constant sets are defined in the form of $k_i = 10^{m_i}$. Starting from the initial guess value for each $m_i$, the time evolutions of the global self-assembly event are traced with giving each $m_i$ a stepwise increment or decrement, searching for smaller and smaller values of the residual sum of squares for both the existence ratios and the *n–k* plot.
2. Initial guess sets are given in several different ways for exploring as broad parameter space as possible. An example is the uniform one with ($m_1$, $m_{-1}$, $m_2$, $m_{-2}$, …) = (0, 0, 0, 0, …). In another guess, rate constants for the oligomerization are given 10 to 100 times larger values than others by intention, by considering that those reactions (especially, the inclusion of the free multitopic ligand L) occur very fast at the onset of the global self-assembly.
3. Additionally, in the parameter search, chemical conditions such as the magnitude relation among the association constants are preliminarily imposed.
4. As a result of the global search, most of $k_i$'s settle into almost definite values, with others floating within relatively wide numerical ranges. From our numerical experiences, the latter constants do not largely affect the global reproduction of the experimental self-assembly process and the dominant reaction pathways. Therefore, for those rate constant parameters, representative values are picked up within the scope of our chemical intuition (At this point an arbitrariness occurs).

As the parameter search is performed in the above procedures for giving a good fit to the QASAP counterpart, we cannot calculate the amounts of statistics such as the standard deviation for the obtained rate constant values. The adequacy of the fitting to the experimental data was evaluated from the residual sum of squares (RSS) with the average of the experimental data, obtained from three runs. For all the time steps $t_i$ at which the experimental data of existence ratios $R_{ex}^S$ and parameters $n_{ave}$ and $k_{ave}$ are available, RSS's are calculated with the numerically obtained values $R_{nu}^S$ as (note that $S = [\boldsymbol{Pd}\text{Py*}_2]^{2+}$, **1**, $[\boldsymbol{Pd}_6\mathbf{1}_3]^{12+}$, or Py*),

$$\text{RSS}_1 = \sum_{t_i}\sum_{S}\left(R_{nu,t_i}^S - R_{ex,t_i}^S\right)^2$$

$$\text{RSS}_2 = \sum_{t_i}\left(\langle n\rangle_{nu,t_i} - \langle n\rangle_{ex,t_i}\right)^2 + \sum_{t_i}\left(\langle k\rangle_{nu,t_i} - \langle k\rangle_{ex,t_i}\right)^2$$

A representative result is shown in Figure 3, in which the initial particles and the volume of the simulation box were set to be a hundred times larger than the rough parameter search, i.e., $\langle[\boldsymbol{Pd}\text{Py*}_2]^{2+}\rangle_0$ = 240,000, $\langle\mathbf{1}\rangle_0$ = 120,000, and $V = 5.0 \times 10^{-16}$ L. Although the numerical results shown there were obtained from a single

numerical run, similar behaviors were found from several runs for the particle numbers given above. From 10 numerical runs, it was found that the $RSS_1 \sim 210$ (the root mean square, $RMS_1$, for total of 84 sample points ~ 1.6) and $RSS_2 \sim 0.27$ ($RMS_2 \sim 0.08$ for 42 sample points). The same procedures were repeated for the ligand **2**, with the initial conditions $\langle[\boldsymbol{Pd}\mathrm{Py}^*_2]^{2+}\rangle_0 = 3{,}000$, $\langle\mathbf{2}\rangle_0 = 1{,}500$, and $\langle\mathrm{others}\rangle_0 = 0$ used for the parameter fitting in the simulation box of $V = 2.5 \times 10^{-18}$ L. Refined calculations after getting the optimal parameter set were performed with $\langle[\boldsymbol{Pd}\mathrm{Py}^*_2]^{2+}\rangle_0 = 300{,}000$, $\langle\mathbf{2}\rangle_0 = 150{,}000$, and $V = 2.5 \times 10^{-16}$ L, and a representative result is given in Figure S6. For the ligand **2**, from 10 numerical runs, it was found that $RSS_1 \sim 1150$ ($RMS_1$, for total of 152 sample points ~ 2.8) and $RSS_2 \sim 0.56$ ($RMS_2 \sim 0.086$ for 76 sample points).

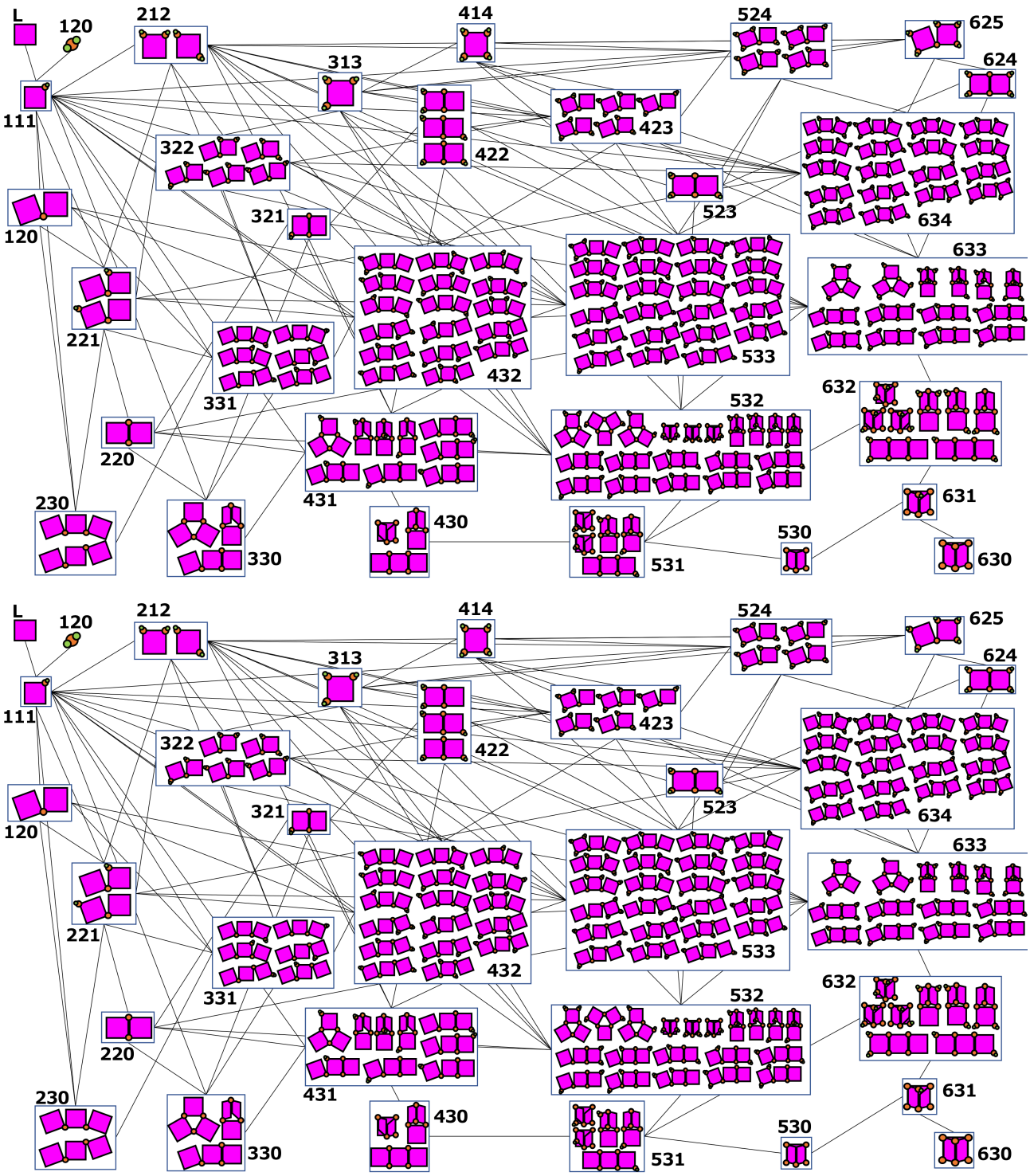


**Figure S4.** All the species consider and a simplified reaction network in NASAP for the self-assembly of the $[\boldsymbol{Pd}_6\mathrm{L}_3]^{12+}$ prisms.

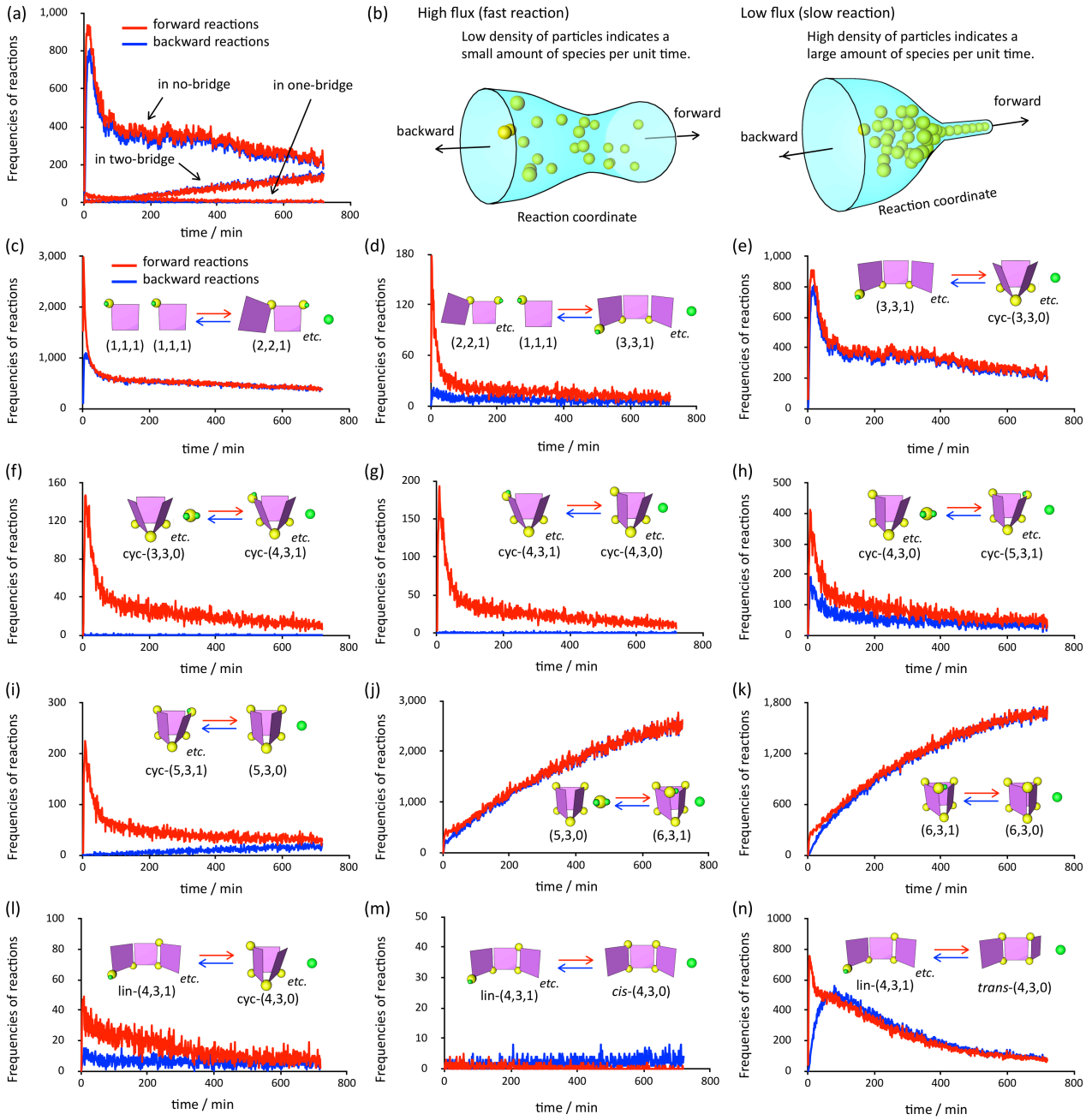


**Figure S5.** Frequencies of the elementary reactions related to the major self-assembly pathway and to the production of the kinetic traps for the $[\boldsymbol{Pd}_6\mathbf{1}_3]^{12+}$ prism. (a) Frequencies of the cyclization reactions in the intermediates with and without bridging(s). (b) Schematic representation of how the frequencies of elementary reactions relate to the reaction rates and the number of species is schematically shown. (c–k) Frequencies of the reactions in the major self-assembly pathway. (l-n) Frequencies of the reactions concerning lin-(4,3,1), indicating that the major reaction of lin-(4,3,1) is the bridging reaction to form *trans*-(4,3,0), which is kinetically trapped.

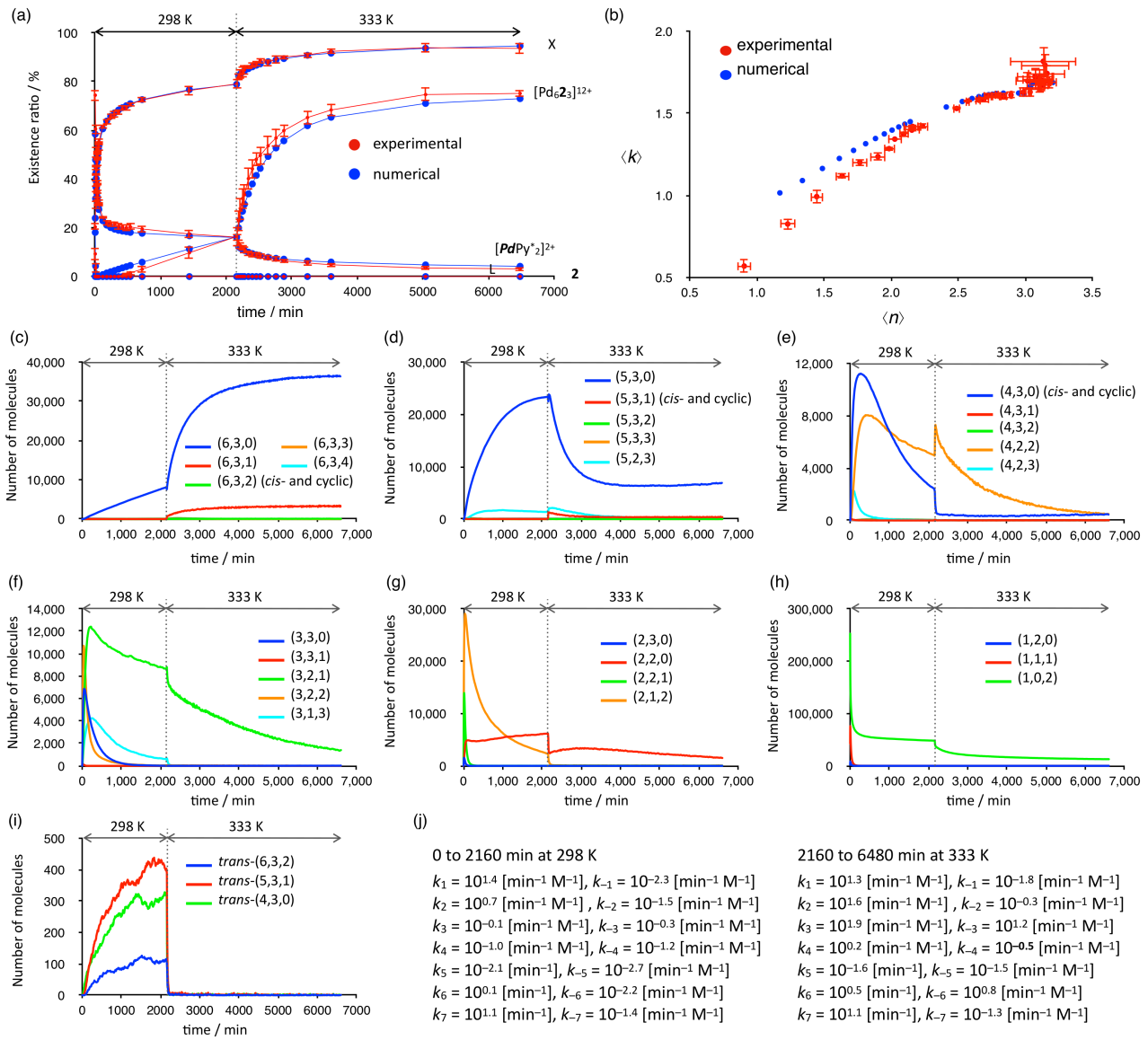


**Figure S6.** (a) Plots of experimental and simulated existence ratios of the substrates and the products for the self-assembly of the $[\boldsymbol{Pd}_6\mathbf{2}_3]^{12+}$ prism. (b) Plots of experimental and simulated ($\langle n \rangle$, $\langle k \rangle$) values for the self-assembly of the $[\boldsymbol{Pd}_6\mathbf{2}_3]^{12+}$ prism. (c–i) The change in the number of species with time for the self-assembly of the $[\boldsymbol{Pd}_6\mathbf{2}_3]^{12+}$ prism simulated with the rate constants obtained by NASAP. (j) The rate constants for the self-assembly of the $[\boldsymbol{Pd}_6\mathbf{2}_3]^{12+}$ prism determined by NASAP. The self-assembly was conducted at 298 K until 36 h (2160 min), after which the reaction mixture was heated at 333 K.

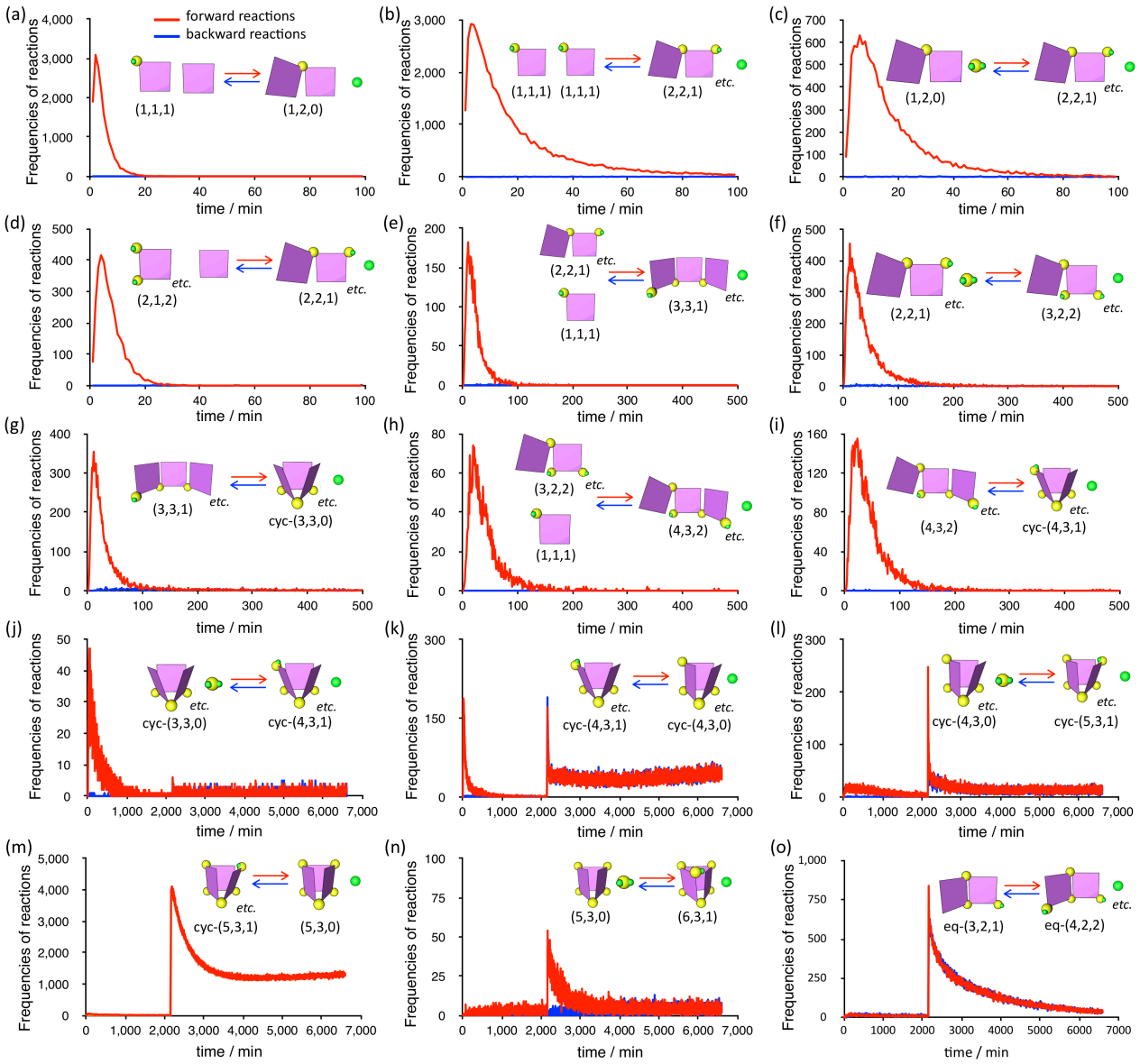


**Figure S7.** Frequencies of the elementary reactions related to the major self-assembly pathway and to the production of the kinetic trap for the $[\boldsymbol{Pd}_6\mathbf{2}_3]^{12+}$ prism. The self-assembly was conducted at 298 K until 36 h (2160 min), after which the reaction mixture was heated at 333 K. (a)-(n) Frequencies of the forward and backward reactions in the major self-assembly pathways. (o) Frequencies of the forward and backward reactions related to the kinetic trap. The self-assembly was conducted at 298 K until 36 h (2160 min), after which the reaction mixture was heated at 333 K.

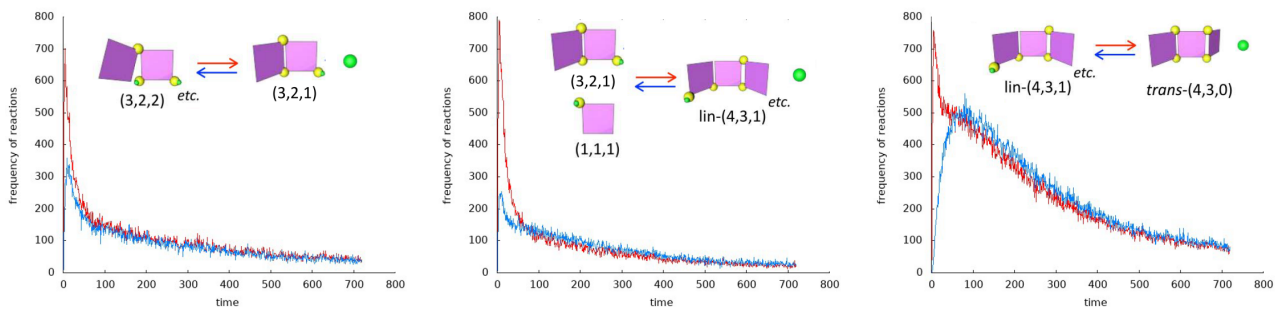


**Figure S8.** The frequencies of the reactions concerning minor self-assembly pathway from (3,2,2) to kinetically trapped *trans*-(4,3,0) for the self-assembly of the $[\boldsymbol{Pd}_6\mathbf{1}_3]^{12+}$ prism (see Figure 1c).

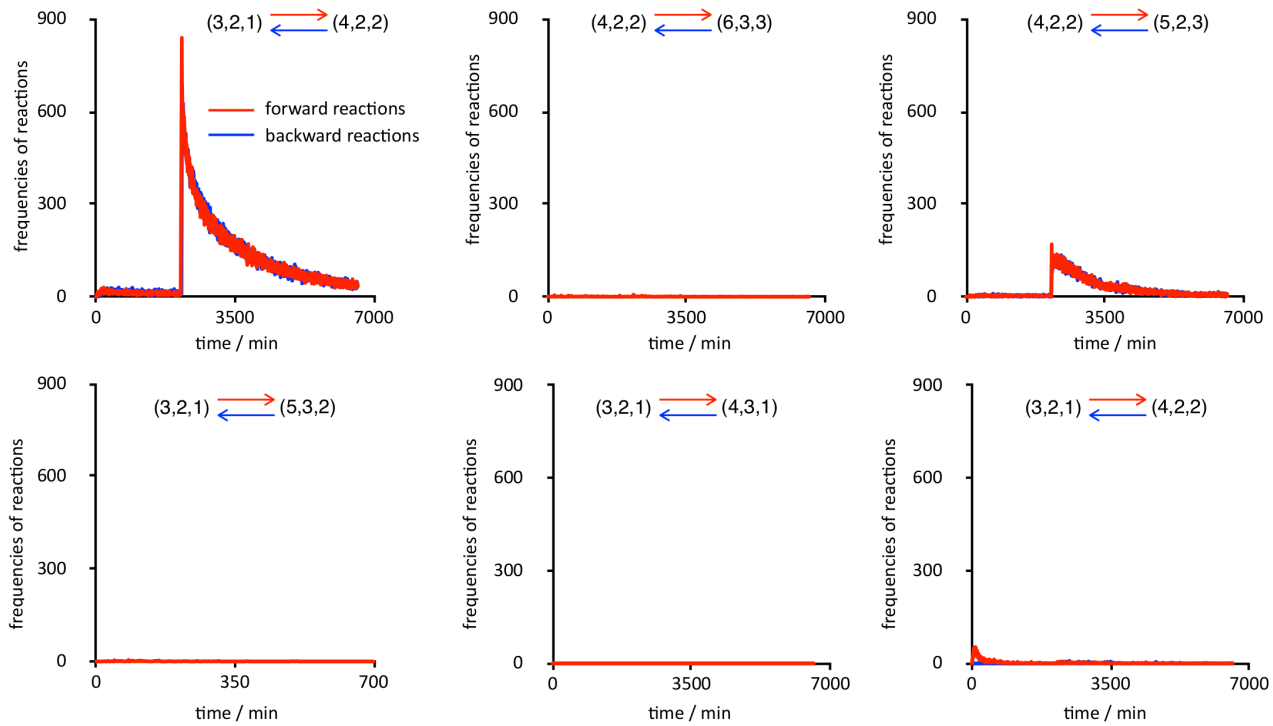


**Figure S9.** The frequencies of the reactions concerning (3,2,1) and (4,2,2) for the self-assembly of the $[\boldsymbol{Pd}_6\mathbf{2}_3]^{12+}$ prism. The self-assembly was conducted at 298 K until 36 h (2160 min), after which the reaction mixture was heated at 333 K.

Monitoring the self-assembly of the $[\boldsymbol{Pd}_6L_3]^{12+}$ prisms by mass spectrometry

**General Procedure**: A solution of $[\boldsymbol{Pd}Py^*_2](BF_4)_2$ ($[Pd]_0$ = 2.0 mM) and ligand **2** ($[\mathbf{2}]_0$ = 1.0 mM) were mixed in a mixed solvent of $CD_3NO_2$ and $CDCl_3$ (4:1, v/v, 600 μL as total). At each time point, 50 μL of the reaction mixture was taken, diluted with $CH_3NO_2$ (500 μL), filtered through a membrane filter (pore size: 0.20 μm), and injected in the mass spectrometer (Measurement condition: Capillary / 1.5 kV; Sampling Cone / 30 V; Source Offset / 80 V; Source / 80 °C; Desolvation / 150 °C; Cone Gas / 50 L $h^{-1}$; Desolvation Gas / 800 L $h^{-1}$) with 5.0 μL $min^{-1}$ flow rate to obtain ESI-TOF mass spectra.

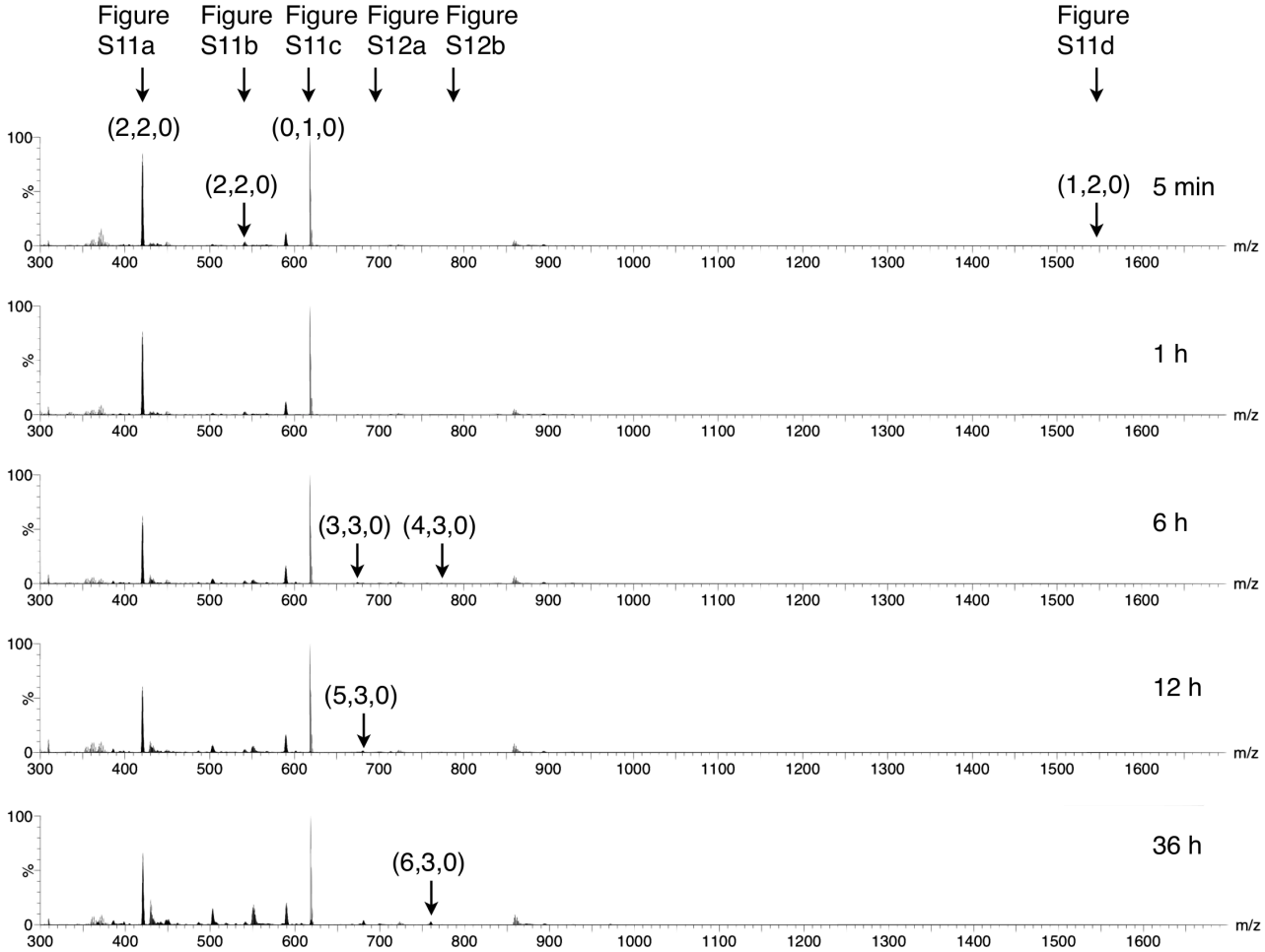


**Figure S10.** ESI-TOF mass spectra of the reaction mixture for the self-assembly of the $[\boldsymbol{Pd}_6\mathbf{2}_3]^{12+}$ prism from $[\boldsymbol{Pd}Py^*_2](BF_4)_2$ ($[Pd]_0$ = 2.0 mM) and **2** ($[\mathbf{2}]_0$ = 1.0 mM) in $CD_3NO_2$ and $CDCl_3$ (4:1, v/v) at 298 K measured at 5 min, 1 h, 6 h, 12 h, and 36 h. *m/z*: 300–1700. (*a*,*b*,*c*) indicates species $[\boldsymbol{Pd}_a\mathbf{2}_bPy^*_c]^{2a+}$.

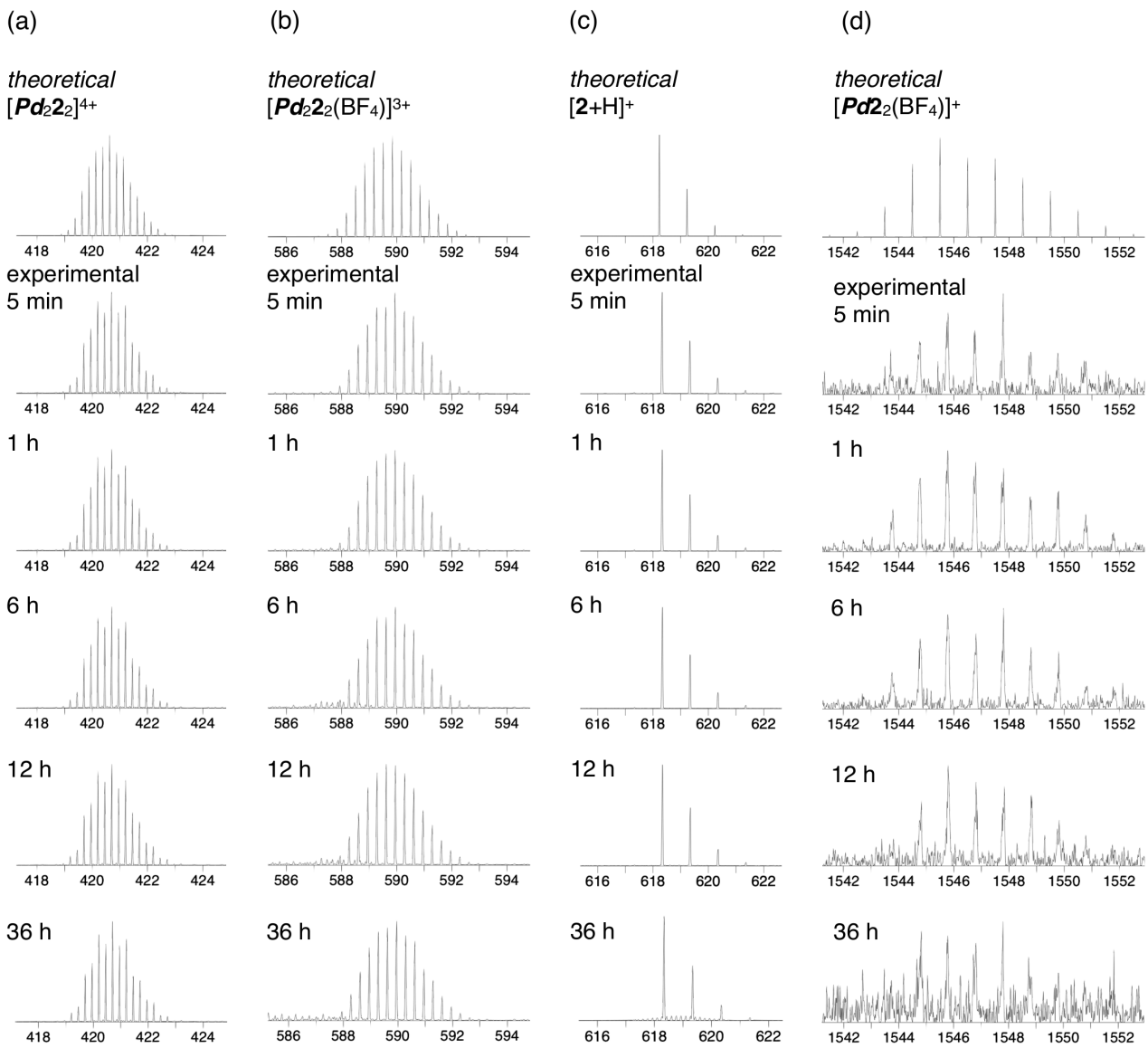


**Figure S11.** Partial ESI-TOF mass spectra of the reaction mixture for the self-assembly of the $[\boldsymbol{Pd}_6\mathbf{2}_3]^{12+}$ prism from $[\boldsymbol{Pd}\mathrm{Py}^*_2](\mathrm{BF}_4)_2$ ($[\mathrm{Pd}]_0$ = 2.0 mM) and **2** ($[\mathbf{2}]_0$ = 1.0 mM) in $CD_3NO_2$ and $CDCl_3$ (4:1, v/v) at 298 K measured at 5 min, 1 h, 6 h, 12 h, and 36 h. (a) $[\boldsymbol{Pd}_2\mathbf{2}_2]^{4+}$, (b) $[\boldsymbol{Pd}_2\mathbf{2}_2(\mathrm{BF}_4)]^{3+}$, (c) $[\mathbf{2}+\mathrm{H}]^+$, and (d) $[\boldsymbol{Pd}\mathbf{2}_2(\mathrm{BF}_4)]^+$.

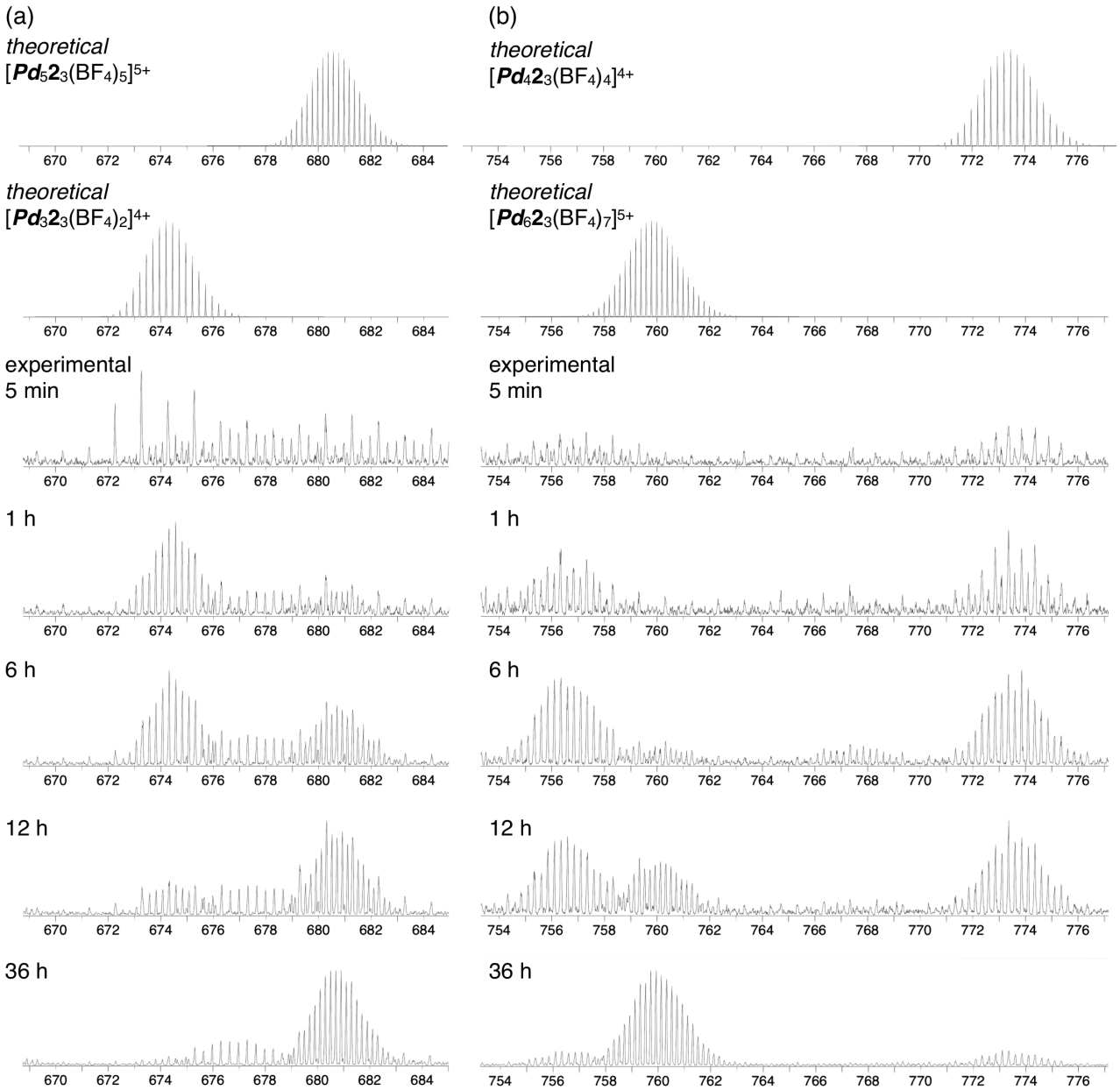


**Figure S12.** Partial ESI-TOF mass spectra of the reaction mixture for the self-assembly of the $[\boldsymbol{Pd}_6\mathbf{2}_3]^{12+}$ prism from $[\boldsymbol{Pd}\mathrm{Py}^*_2](\mathrm{BF}_4)_2$ ($[\mathrm{Pd}]_0$ = 2.0 mM) and **2** ($[\mathbf{2}]_0$ = 1.0 mM) in $CD_3NO_2$ and $CDCl_3$ (4:1, v/v) at 298 K measured at 5 min, 1 h, 6 h, 12 h, and 36 h. (a) $[\boldsymbol{Pd}_5\mathbf{2}_3(\mathrm{BF}_4)_5]^{5+}$ and $[\boldsymbol{Pd}_3\mathbf{2}_3(\mathrm{BF}_4)_2]^{4+}$, and (b) $[\boldsymbol{Pd}_4\mathbf{2}_3(\mathrm{BF}_4)_4]^{4+}$ and $[\boldsymbol{Pd}_6\mathbf{2}_3(\mathrm{BF}_4)_7]^{5+}$.

## References


1. Chakraborty, R.; Sahoo, S.; Halder, N.; Rath, H.; Chattopadhyay, K. *ACS Chem. Neurosci.* **2019**, *10*, 573–587.
2. He, Z.; Li, M.; Que, W.; Stang, P. J. *Dalton Trans.* **2017**, *46*, 3120–3124.
3. Komine, S.; Takahashi, S.; Kojima, T.; Sato, H.; Hiraoka, S. *J. Am. Chem. Soc.* **2019**, *141*, 3178–3186.
4. Tateishi, T.; Takahashi, S.; Okazawa, A.; Martí-Centelles, V.; Wang, J.; Kojima, T.; Lusby, P. J.; Sato, H.; Hiraoka, S. *J. Am. Chem. Soc.* **2019**, *141*, 19669–19676.